FORMATION OF KETENIMINIUM SALTS: MECHANISTIC ASPECTS AND EFFECT OF SUBSTITUENTS

by

Zeynep Aktaş

B.S., Chemistry, Istanbul Technical University, 2018

Submitted to the Institute for Graduate Studies in
Science and Engineering in partial fulfillment of
the requirements for the degree of
Master of Science

Graduate Program in Chemistry

Boğaziçi University

2020

ACKNOWLEDGEMENTS

First and foremost, I would like to thank my advisor, Assoc. Prof. Şaron Çatak, for her guidance, encouragement, support, and understanding throughout my master years. I have gained valuable information and golden experience from her.

I wish to extend my appreciation to my thesis committee members: Assoc. Prof. Ersin Acar and Assist. Prof. Burcu Dedeoğlu.

This study has been supported by TUBITAK Project No. 115Z738. I acknowledge TUBITAK ULAKBIM High Performance Computing Center for computational resources.

I thank all members of CCBG lab for their support and sincere friendship. Especially, I would like to thank my friends Beyza Horoz, Busenur Aslanoğlu, Gamze Tanrıver, Pelin Ulukan, İpek Munar, Başak Koca, Öyküm Naz Avcı, Aslıhan Hepgüler. Our quick coffee breaks, fun lunch parties, endless gossip sessions and even online Turkish coffee meetings was the best part of my master's years.

Kerem Engin, I would also thank you for being my biggest supporter. When I doubt about myself, you gave me strength and encouragement to move forward. I am the luckiest person to have you in my life.

Finally, I wish to thank my parents and my siblings for their eternal love and endless support. I dedicate my thesis to my beloved family.

Abstract

FORMATION OF KETENIMINIUM SALTS: MECHANISTIC ASPECTS AND EFFECT OF SUBSTITUENTS

Most organic reactions occur in several consecutive steps that include the generation of highly reactive intermediates, which are short-lived. Keteniminium salts (KI) are key and versatile intermediates in synthetic organic chemistry that are used in various reactions, such as [2+2] and [4+2] cycloadditions, Pictet–Spengler cyclization, Claisen-like rearrangements. Elucidation of the mechanistic aspect of these KI formation reactions ensures the understanding of the formation of this intermediate. In this study, to provide a comprehensive understanding of the KI formation, various formation mechanisms were investigated, using density functional theory (DFT). Particularly, Ghosez's formation mechanism was extensively elaborated since Ghosez's reaction occurs in mild conditions and is the most frequently used experimental method. Moreover, a broad range of substituents was examined to give perspective to the possible contributions of the substituents. The effect of these substituents on the reactivity of starting amides was also inspected using population analysis, distortion/interaction-activation strain model analysis, non-covalent interaction (NCI) analysis. In the final part of the study, the substituent effect on corresponding KIs is also investigated in the frame of Conceptual DFT. Computed data showed that, in general, electron-donating groups (EDGs) decrease the activation barrier by increasing the electron density of the amide carbonyl oxygen in contrast to electron-withdrawing groups (EWGs). Besides, according to the distortion/interaction-activation strain model and NCI analysis, electronic and steric effects are notable factors on electrophilic activation of the starting amide during KI formation. This study will contribute a pivotal insight into the mechanistic aspects of the KI formation and the role of the substituents.

ÖZET

KETENİMİNYUM TUZLARININ OLUŞUMU: MEKANİSTİK ÖZELLİKLER VE SÜBSTİTÜENT ETKİSİ

Organik reaksiyonların çoğu, kısa ömürlü ve oldukça reaktif olan ara ürünlerin oluşumunu içeren birkaç ardışık adımda meydana gelir. Keteniminium tuzları (KI), sentetik organik kimyada [2+2] ve [4+2] siklokatılma, Pictet-Spengler siklizasyonu, Claisen düzenlemeleri gibi çeşitli reaksiyonlarda kullanılan anahtar ve çok yönlü ara maddelerdir. KI oluşum reaksiyonlarının mekanik yönünün aydınlatılması, bu ara maddenin oluşumunun anlaşılmasını sağlar. Bu çalışmada, KI oluşumunun kapsamlı bir şekilde anlaşılmasını sağlamak için, bir yoğunluk fonksiyonel teorisi (DFT) kullanılarak çeşitli oluşum mekanizmaları araştırılmıştır. Ghosez'nin reaksiyonu hafif koşullarda meydana geldiğinden ve en çok kullanılan deneysel yöntem olduğundan, Ghosez'nin oluşum mekanizması kapsamlı bir şekilde detaylandırılmıştır. Ayrıca, sübstitüentlerin olası katkılarına perspektif sağlamak için geniş bir sübstitüent yelpazesi incelenmiştir. Bu sübstitüentlerin başlangıç amidlerinin reaktivitesi üzerindeki etkisi, popülasyon analizi, distorsiyon/etkileşim-aktivasyon modeli analizi, NCI analizi kullanılarak da incelenmiştir. Çalışmanın son bölümünde, karşılık gelen KI'lar üzerindeki sübstitüent etkisi de Kavramsal DFT çerçevesinde incelenmiştir. Hesaplanan veriler, genel olarak elektron veren grupların (EDG), elektron çeken gruplara (EWG) nazaran amidlerin karbonil oksijeninin elektron yoğunluğunu artırarak aktivasyon bariyerini azalttığını gösterdi. Ayrıca, distorsiyon/etkileşim-aktivasyon gerinim modeline ve NCI analizine göre, elektronik ve sterik etkiler, KI oluşumu sırasında başlangıç amidinin elektrofilik aktivasyonu üzerinde dikkate değer faktörlerdir. Bu çalışma, KI oluşumlarının mekanik yönüne ve sübstitüentlerin rolüne ilişkin önemli bir kavrayışa katkıda bulunacaktır.

Contents

List of Figures

List of Tables

LIST OF SYMBOLS

E_{el}	Electronic Energy
$\mathrm{E_c}[\rho]$	Correlation Energy
$\mathrm{E_x}[\rho]$	Exchange Energy
eV	Electron Volt
$f(r)$	Fukui Function
H	Hamiltonian Operator
h_{KS}	Kohn-Sham Hamiltonian Operator
$\mathrm{J}[\rho(\mathrm{r})]$	Coulomb Energy
$P(r)$	Parr Function
q_A	Atomic Charge
$\mathrm{T}[\rho(r)]$	Kinetic Energy of Interacting Electrons
$\mathrm{T}_{ni}[\rho(r)]$	Kinetic Energy of Non-interacting Electrons
$V_{ext}(r)$	External Potential
$V_{ee}[\rho(r)]$	Electron-Electron Interactions
Z	Atomic Number
$\Delta\mathrm{E}^{\ddagger}$	Electronic Activation Energy
$\Delta\mathrm{E}_{dist}$	Distortion Energy
$\Delta\mathrm{E}_{int}$	Interaction Energy
$\Delta\mathrm{G}^{\ddagger}$	Gibbs Free Energy of Activation
$\Delta\mathrm{G}_{rxn}$	Gibbs Free Energy of Reaction
ε	Dielectric Constant
$\rho(\mathrm{r})$	Electron Density
ϕ_s	Quantitative Topological Descriptor
Ψ	Many Electron Wavefunction

LIST OF ACRONYMS/ABBREVIATIONS

ASM	Activation Strain Model
B3LYP	Becke-3-parameter Lee-Yang-Par functional
DFT	Density Functional Theory
EDG	Electron-Donating Group
EWG	Electron-Withdrawing Group
GGA	Generalized Gradient Approximation
GTO	Gaussian Type Orbital
HF	Hartree-Fock Theory
HOMO	Highest Occupied Molecular Orbital
IRC	Intrinsic Reaction Coordinate
KI	Keteniminium Salt
LDA	Local Density Approximation
LUMO	Lowest Unoccupied Molecular Orbital
M06-2X	Hybrid Meta Exchange-Correlation Functional
MPW1K	Modified Perdew-Wang 1-parameter Model for Kinetics
NAO	Natural Atomic Orbitals
NBO	Natural Bond Orbitals
NCI	Non-covalent Interactions
NPA	Natural Population Analysis
PC	Product Complex
PCM	Polarizable Continuum Model
PRC	Pre-reactive Complex
SCF	Self Consistent Field
STO	Slater Type Orbital
TCE	Tetracyanoethylene
TS	Transition State
ωB97xD	Long-Range Corrected Hybrid Functional with Dispersion Correction

1. INTRODUCTION

The majority of organic reactions proceed through short-lived, high-energy, and reactive intermediates. Since the conversion of these reactive intermediates to more stable molecules underlies most of the transformation, they are at the center of organic synthesis. In addition, they are beneficial in understanding the mechanism and selectivities of reactions. They can be simply classified as cationic, ionic, and radical species other than their neutral and metal including types. The cationic type of intermediates draws attention since the chemistry of carbocations leads to many developments in chemical synthesis. Apart from pure carbocations, carbocation intermediates include oxonium and iminium along with ketenium and keteniminium ions [1]. Keteniminium salts (KI) which are nitrogen analogues of ketenes are highly reactive cationic intermediates. They are considered superior to ketens since they are more stable, reactive, and regioselective, in addition to not giving any side reactions, for instance, polymerization or dimerization [1, 12]. KIs are used in various reactions as intermediates, such as [2+2] and [4+2] cycloadditions [2, 13], Pictet–Spengler cyclizations [14], cyclization of ortho-vinyl-anilino-amides [15], and $6\pi/10\pi$ electrocyclizations [16–21].

The formation reactions of these unique intermediates are first mentioned in 1967 [7] by Viehe et al. Nevertheless, these formation reactions have some disadvantages, such as usage of toxic phosgene gas and undesired side reactions of KI salts with their precursors. The expansion of the application area and the discovery of the new formation reactions of keteniminium salts required further investigation about the chemistry of these structures. Therefore, Ghosez and coworkers [5] introduced a formation method, which is synthetically the most useful one in, 1981. Several formation reactions (Figure 1.1) have been proposed up to now as well as Ghosez's mechanism. These are methylation of ketenimines [6], reactions of a-halo enamines with Lewis acids [2, 4], protonation of ynamines [1, 17, 21], and ynamides [8–10].

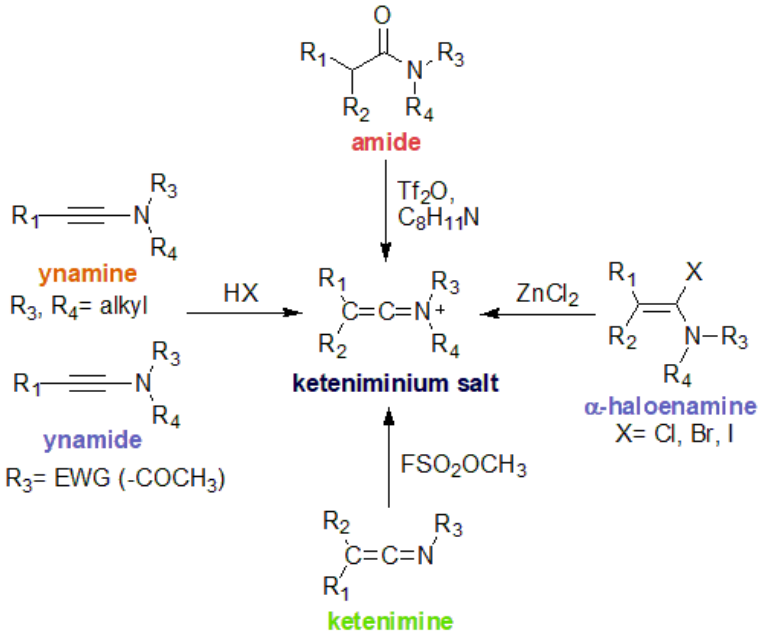

Figure 1.1. Various formation reactions of KI [1–10]

1.1. Generation of Keteniminium Salts via Ghosez's Mechanism

Keteniminium salt formation was first observed in the preparation of alkyl and aryl-substituted α-chloroenamines from tertiary amides [3] by Viehe and Ghosez *et.al.* These KI are in equilibrium with obtained α-chloroenamines (Figure 1.2). Later, Viehe and Ghosez *et. al* reported that α-chloroenamines readily give cycloaddition reactions with olefins and acyclic dienes to generate cyclobutenone derivatives [2, 4] in high yields. They stated that this exceptional reactivity is due to the equilibrium of α-chloroenamines with keteniminium salts, which reacts with the nucleophilic agents to give cycloaddition reactions.

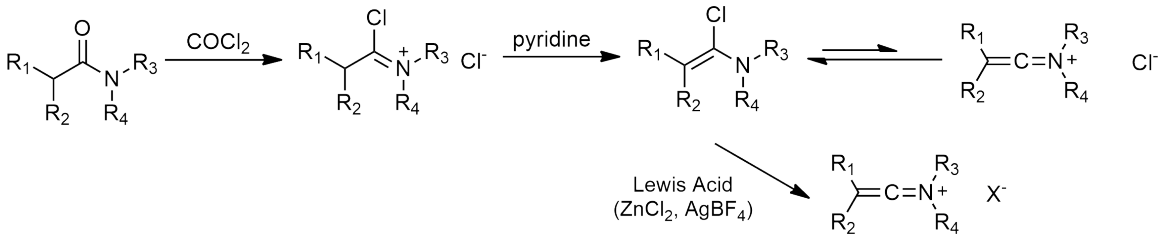

Figure 1.2. Viehe's method for generation of keteniminium salts [3].

Furthermore, these keteniminium salts were used in synthesis of four-membered rings via cycloaddition reactions [2,4,22]. However, Viehe's formation method had some limitations. Although keto keteniminium salts were readily generated from the reaction of α-chloro enamines with Lewis acids, aldo keteniminium salts reacted faster with their precursors and gave side products due to notable nucleophilicity of the starting material, α-chloroenamines. This undesired side reaction could be prevented by the formation of KI from non-nucleophilic α-substituted enamine intermediates [1, 5, 11]. Based on these limitations, Ghosez reported an alternative method for the generation of keteniminium salts starting from amides [5], which became the most widely used procedure. The reaction mechanism consists of three consecutive steps. The first step is the electrophilic activation of the amide with triflic anhydride providing a transient O-triflyliminium triflate, which at the second step, upon reaction with collidine, gives the corresponding α-trifloylenamine; the enamine then undergoes elimination to the desired keteniminium triflate at the last step [1] (Figure 1.3).

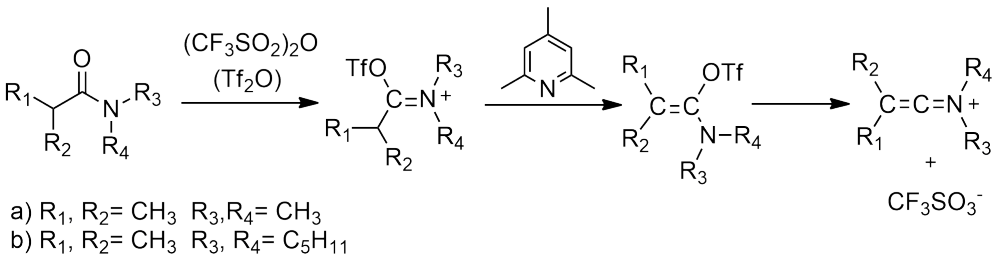

Figure 1.3. Ghosez's formation reaction of keteniminium salts [5].

By using triflic anhydride (Tf_2O) and the non-nucleophilic collidine base for amide activation, the nucleophilicity of α-trifloylenamine precursors is lowered, which suppresses the dimerization reactions. In this case, since nucleophilicity of TfO^- ion is lower than Cl^-, the equilibrium between the α-trifloylenamine precursor and the KI favors the formation of KI. In addition, collidine is chosen since using a hindered base slows down the reaction of KI with its precursor [5]. Furthermore, readily available amides does not require an isolation in the case of α-chloroenamines and so they can be used directly as a starting material [11].

As a consequence, both aldo and keto keteniminium salts gave cycloaddition reactions with olefins generally with moderate yields. Additionally, keteniminium salts were proved to be superior to their corresponding ketenes, since ketenes only react with activated alkenes or alkynes [5]. However, Snider's study on [2+2] cycloaddition of ketenes and keteniminium salts showed that in a series of starting materials, ketenes outperformed their corresponding KI. Later on, Brady concluded that while keto ketenes gave better yields than keto keteniminium salts in [2+2] cycloaddition reactions, aldo keteniminium salts are superior to aldo ketenes [23].

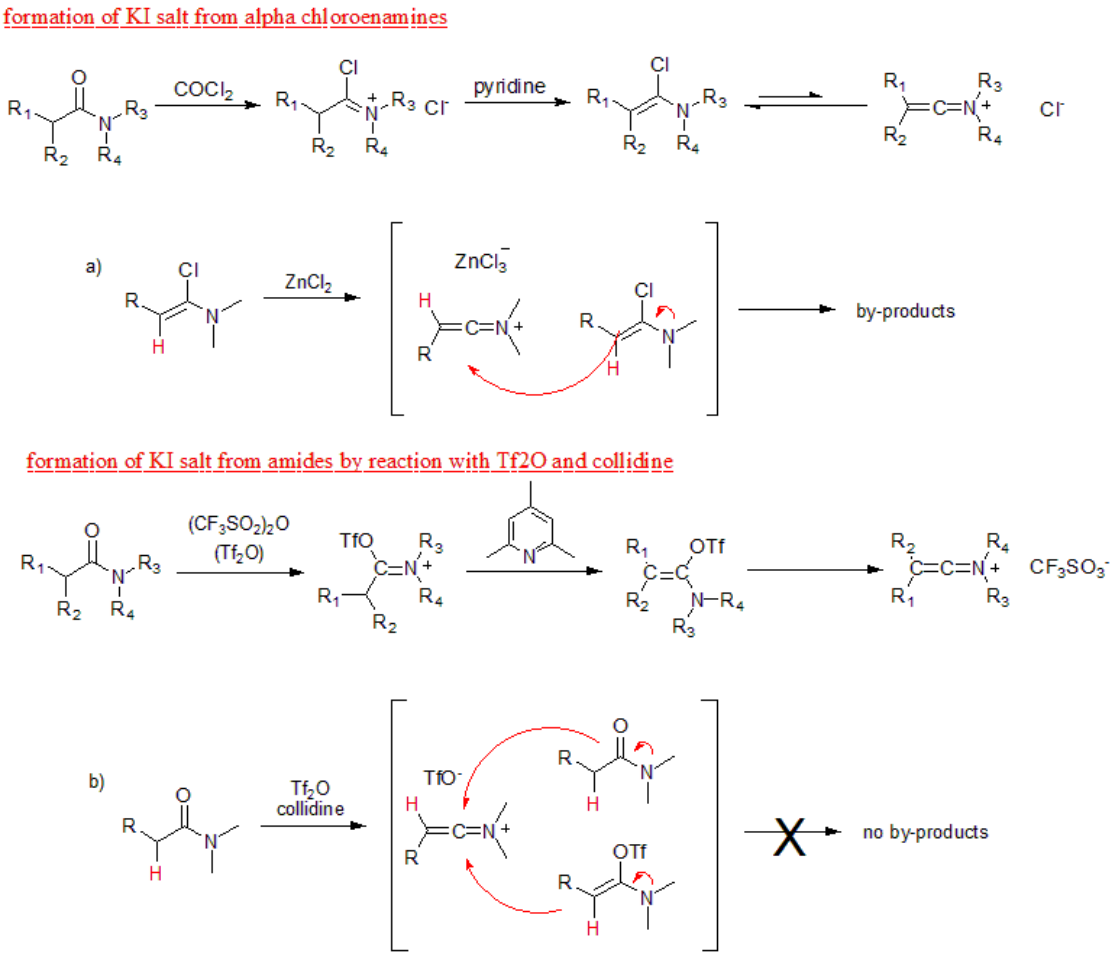

Figure 1.4. Reactivity difference between aldo keteniminiums generated from α-chloroenamines and amides [11].

1.2. Generation of Keteniminium Salts from α-halo Enamines

As previously mentioned, Viehe showed that α-chloroenamines could easily be added to acetylenes to give cyclobutanones derivatives via [2+2] cycloaddition reactions [3]. It is claimed that the ease of reaction stems from the equilibrium between α-chloroenamines and keteniminium salts. Further investigations about α-chloroamines, their preparation and reactivity in [2+2] reactions proceeded by Ghosez in 1972. They reported that upon replacing the carbonyl group in ketenes by an immonium, the resulting keteniminium intermediate becomes more effective in [2+2] cycloaddition reactions. Reaction conditions are milder, the yield is higher, and the starting material is cheaper. This showed that keteniminium salts are more preferable than their corresponding ketene analogs [2]. Aforementioned α-chloroenamines are versatile synthetic intermediates obtained from the activation of amides with phosgene and a Schiff base that is in equilibrium with the corresponding keteniminium salt [1]. Although the equilibrium favors chloroenamine, the use of Lewis acids such as silver tetrafluoroborate ($AgBF_4$) and/or zinc chloride ($ZnCl_2$) prefers the formation of the keteniminium ion [2,3]. Ghosez group developed a procedure for keteniminium salt formation in presence of $ZnCl_2$ since $AgBF_4$ is an expensive reagent [4]. Even though this is an effective generation method for keteniminium salts, the procedure includes using highly toxic gas, phosgene, in order to obtain the starting material α-chloroenamine. Moreover, the aldo keteniminium salts readily react with their precursors as mentioned earlier.

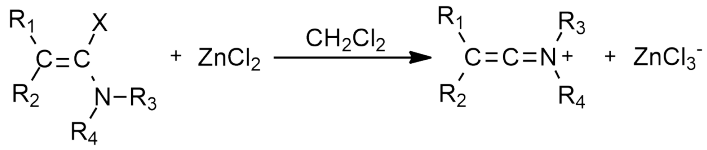

Figure 1.5. Reactivity difference between aldo keteniminiums generated from α-chloroenamines and amides [4].

1.3. Generation of Keteniminium Salts from Ketenimines

In 1975, Deyrup also proposed an alternative route to obtain functionally substituted aziridines synthesis from ring closure of azomethine ylides by deprotonation of iminium salts [24]. In this regard, a series of iminium salts were generated by alkylation of imines with methyl fluorosulfonate. Methyl fluorosulfonate, which is a highly reactive direct alkylation agent was chosen, since it consists of a methyl group with methyl cation ($^{+}$CH3) characteristics and an excellent leaving group, (FSO_2O^{-}). Comparative studies on the alkylating ability of methyl fluorosulfonate indicates that it is indeed one of the direct alkylation agents since it reacts with the majority of lone pair bearing functional groups. Amines also undergo quaternization with methyl fluorosulfonate [25]. In addition, the dealkylation of iminium salts was a major problem for this reaction since it could compete with the deprotonation process. By using methyl fluorosulfonate, the product anion could be relatively non-nucleophilic and would not lead to dealkylation. The resulting iminium salts are relatively stable and the iminium salt bearing *t*-Bu substituents were purified sufficiently [24]. After the successful generation of azomethine ylide *via* deprotonation of iminium salts, Deyrup tried to extend this study to keteniminium salts. Although the alkylation of ketenimines with methyl fluorosulfonate (magic methyl) led to the successful generation of keteniminium salts (Figure 1.6), these salts were highly reactive for deprotonation studies. In the subsequent deprotonation step, the KI preceding keteniminium salts dimerized to piperazine instead of the intended aziridine. Nevertheless, although deprotonation did not lead to the desired aziridine structures, a new KI formation method was discovered [6]. Despite being an excellent direct alkylating agent, the use of methyl fluorosulfonate, is an extremely toxic substance inducing chronic and long-term effects, which is a disadvantage for this formation method.

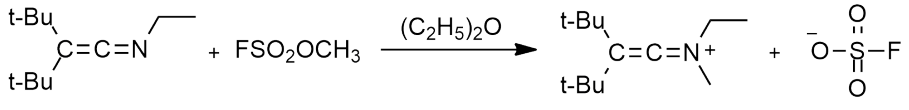

Figure 1.6. Generation of KI salts from methylation of ketenimines [6].

1.4. Generation of Keteniminium Salts from Ynamines and Ynamides

The most versatile and unique subclass of alkynes is the heteroatom-substituted ones. Ynamines are inherently highly reactive heteroatom-substituted alkynes, which have a nitrogen atom directly bonded to the triple bond. Their reactivity is based on the electron-donating ability of the nitrogen atom, which polarizes the triple bond [26]. However, their sensitivity towards hydrolysis brings many difficulties to their preparation and handling, which limits their synthetic use. Thus, an electron-withdrawing group (EWG) on the nitrogen atom greatly enhances the stability of ynamines. This electron-deficient type of ynamines called ynamides still have a strong polarization of the triple bond, although tempered by the electron-withdrawing group [8, 10]. Keteniminium salts are the intermediates in both the synthesis of ynamines from α-halogeno iminium salts and reactions of ynamines with protonic acids, alkylating agents and ketenes [3, 27]. As the protonation of ynamines give reactive KI intermediates, trapping it with water leads to simple amides in an expensive way due of their hydrolytic instability [8]. In addition to the previously mentioned formation methods of the "classical" keteniminium salts from ynamines, protonation of ynamides is the source of "activated" keteniminium salts [1, 10, 26, 27]. The reason why these ynamide-based keteniminium salts are called "activated" is because they are substituted with an electron-withdrawing group on the nitrogen atom, making them more reactive. Since they have easily tuned and controlled reactivity, the activated keteniminium salts can promote the reactions that classical ones may fail, such as activating poorly reactive C-H bonds through hydrogen shift and hydride abstraction [27]. This method includes the reaction of ynamines and ynamides with the several electrophiles. The electrophiles used in these keteniminium formation reactions can be classified into five categories as acids, halogenium ions, chalcogenyl halides, C-electrophiles, and electrophilic metal complexes. Strong acids are generally used for protonation of ynamines and ynamides. Moreover, it is important to choose a suitable electrophile, which does not react with the EWG on the ynamide, but reacts with nucleophilic nitrogen atom [1].

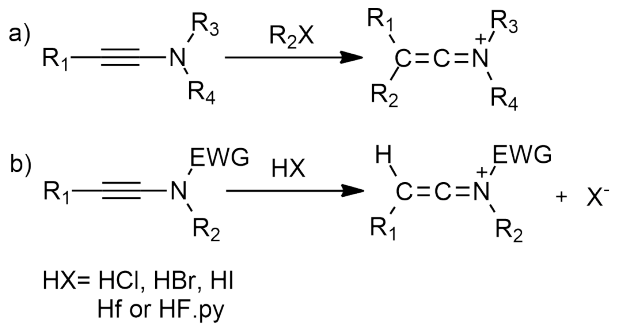

Figure 1.7. Generation of KI salts from a) ynamines and b) ynamides. [1]

1.5. Aim of the Study

In this thesis, the main purpose is to computationally rationalize the formation reactions of keteniminium salts, examine the substituent effect on Ghosez's formation reaction and investigate keteniminium salt reactivities using a DFT approach. In this regard, the aforementioned four different methods for the formation reactions of keteniminium salts are examined; These are mechanisms of Ghosez's keteniminium salt formation reaction (formation from tertiary amides), alkylation of corresponding ketenimines, reactions of *a*-halo enamines with Lewis acids, and protonation of ynamine and ynamides. To the best of our knowledge, this study is the first computational study to elucidate the possible KI formation mechanisms. These reactions have been modeled and compared with each other to find the most likely mechanism for the formation of keteniminium salts. In the second part of the study, a wide range of substituents were selected and thoroughly examined to explain their potential contribution to the formation of KIs through Ghosez's mechanism. Reactivity of starting amides with various substituents were evaluated using population (NBO) analysis. In addition, distortion/interaction, critical distances and non-covalent interaction analyses were performed to rationalize the substituent effect. Finally, reactivity of corresponding KIs with several substituents were examined.

2. METHODOLOGY

The main focus of quantum chemistry is the behavior of electrons under the electromagnetic field that arises from the nuclear charge. While classical mechanics depicts systems through specifying velocities and positions, quantum mechanics uses a mathematical vector named wavefunction that theoretically contains all the information about a given system. All properties of this given system can be described by solving Schrödinger's equation

$$H\psi = E\psi \tag{2.1}$$

where H represents the Hamiltonian operator, E stands for the total energy of the system, and ψ corresponds to the wave function. H operator consists of kinetic and potential energy terms of the nuclei and the electrons

$$H = -\sum_i \frac{\hbar^2}{2m_e}\nabla_i^2 - \sum_k \frac{\hbar^2}{2m_k}\nabla_k^2 - \sum_i \sum_k \frac{e^2 Z_k}{r_{ik}} + \sum_{i<j} \frac{e^2}{r_{ij}} + \sum_{k<l} \frac{e^2 Z_k Z_l}{r_{kl}} \tag{2.2}$$

where the electrons are symbolized with i and j , nuclei as k and l masses of nuclei and electron as m_k and m_e, respectively. $\hbar$ in the "h/2π " symbolizes Planck's constant,, e is the electron charge, Z is atomic number r is the distance between the particles and ∇^2 is the Laplacian operator. The kinetic energy of the nuclei and electrons are represented by the first and second terms, respectively. The potential energy stems from Coulomb interactions of nucleus-electron (U_{ik}), electron-electron (U_{ij}), and nucleus-nucleus (U_{kl}) are also represented. However, Schrödinger's equation is not accurate for many-particle systems because of the associative motions of particles. The nuclei are much heavier than the electrons within an atom that leads it to move slower compared to electrons that move and respond to forces quickly.

In addition to this difference, there are attractive forces due to the opposite charges of nuclei and electrons. The Born-Oppenheimer (BO) approximation [28] proposes to separate the motion of the nuclei and electrons of the atom, neglects the motion of the nuclei and considers it stationary, and eliminates the nucleus-electron attraction. As a result of this approximation, the Hamiltonian operator becomes

$$H_{el} = E_k^{kin} + U_{ki} + U_{ij}. \tag{2.3}$$

Thus, the Schrödinger equation with respect to the Born-Oppenheimer approximation becomes,

$$(H_{el} + V_{nn})\psi_{el} = E_{el}\psi_{el} \tag{2.4}$$

where V_{nn} represents the nuclear-nuclear repulsion energy constant, and the eigenvalue E_{el} is the electronic energy. While Schrödinger's equation can define approximately all properties of systems, it is complicated to solve. The solution can be obtained precisely for hydrogen-like systems. Schrödinger equation can be used for all other systems by using the variational principle. Multiplying both sides of Equation 2.1 by ψ gives

$$\psi H \psi = \psi E \psi. \tag{2.5}$$

For many electron systems, integration of both sides in a volume ($d\tau$) gives:

$$E = \frac{\int \psi H \psi d\tau}{\int \psi^2 d\tau}. \tag{2.6}$$

According to this theorem, calculated energy (E) can be equal or greater than the ground state energy E_0. It gives an approximate solution to Schrödinger's equation. In this thesis, Density Functional Theory [29] is utilized as it is considered the most sufficient approach. The theory of DFT will be explained in the next section.

2.1. Density Funtional Theory

Density Functional Theory (DFT) [29] is a commonly used quantum chemistry approach, which was proposed by Hohenberg and Kohn [30,31] in 1964. This approach is based on the Hohenberg-Kohn Existence Theorem [32] which suggested that the wavefunction is determined if the density of the corresponding system is known, so it gives the solution of the Schrödinger equation to obtain energy. The electronic structure of molecules are also calculated with this theorem. Hohenberg and Kohn also prove that external potential V(r) is correlated with electron density ρ(r)

$$\rho(r) : N \int ... \int |\Psi(r_1, r_2, ...r_n)|^2 dr_1 dr_2 ... dr_n \tag{2.7}$$

where r_{i} stands for coordinates of the electrons.

Hohenberg-Kohn Variational Theorem states that when the charge density is in the ground state, the energy content reaches its minimum value. According to this theorem, the ground state electronic energy is a function of the electron density function and represented as

$$E[\rho(r)] = \int V(r)\rho(r)dr + T[\rho(r)] + V_{ee}[\rho(r)] \tag{2.8}$$

where T[ρ(r)] is the kinetic energy of interacting electrons and $\mathrm{V}_{ee}[\rho(\mathrm{r})]$ represent the interelectronic interaction energy. Equation 2.7 can be rewritten with concept for non-interacting electrons presented by Kohn and Sham [33]

$$E[\rho(r)] = \int V(r)\rho(r)d(r) + T_{ni}[\rho(r)] + J[\rho(r)] + E_{XC}[\rho(r)] \tag{2.9}$$

where J[ρ] and, $\mathrm{T}_{\mathrm{ni}}[\rho]$ represents the Coulomb energy and the kinetic energy of the non-interacting electrons and $\mathrm{E}_{\mathrm{XC}}[\rho]$ denoting the exchange-correlation energy functional.

The Coulomb energy of electron-electron interactions is represented as

$$E_{XC}[\rho(r)] = \int \rho(r)\epsilon_{XC}(\rho(r))dr. \tag{2.10}$$

The independent orbitals ψ_i, called as Kohn-Sham orbitals are established by solving the Kohn-Sham equations

$$h_i^{KS}\chi_i = \varepsilon_i\chi_i. \tag{2.11}$$

The Kohn-Sham Hamiltonian $\hbar_i$, is defined as

$$h_i^{KS} = -\frac{\nabla^2}{2} - \sum_k^M \frac{Z_k}{|r_i - r_k|} + \int \frac{\rho(r)}{r_{ij}}dr + V_{XC} \tag{2.12}$$

where V_{XC} represents the exchange-correlation potential and is related to exchange correlation energy by

$$V_{XC} = \frac{\delta E_{XC}}{\delta\rho}. \tag{2.13}$$

V_{XC} is divided into two: an exchange functional and a correlation functional:

$$E_{XC}[\rho] = E_X[\rho] + E_C[\rho] \tag{2.14}$$

The correlation term is related with the interactions between the electrons of opposite spin, while the exchange term is associated with the interactions between the electrons of same spin. The exact form of exchange-correlation energy is unknown.

2.2. Functionals

Since the exact exchange-correlation term is not known, several approximations were invented as DFT developed to determine the approximate exchange-correlation term. Local Density Approximation (LDA) is the first approximation to determine E_{XC}. According to this approach, the electron density of a given system is equal in each site, as uniform gas, and with electrostatic energy of positive charge E_b added, the system becomes neutral. The energy expression is

$$E[\rho] = T_{ni}[\rho] + \int \rho(r)v(r)dr + J[\rho] + E_{xc}[\rho] + E_b. \tag{2.15}$$

Since electron density and positive charge density is equal, the equation can be reduced to

$$E[\rho] = T_{ni}[\rho] + E_{xc}[\rho]. \tag{2.16}$$

E_{xc} can be written as divided into two functionals: an exchange functional and a correlation functional, respectively

$$E[\rho] = T_{ni}[\rho] + E_x[\rho] + E_c[\rho] \tag{2.17}$$

where kinetic energy functional $T_{ni}[\rho]$ is

$$T_{ni}[\rho] = C_F \int \rho(r)^{5/3}dr \tag{2.18}$$

C_F is a constant equal to 2.8712. The exchange functional can be found by using the following equation

$$E_x[\rho] = -C_x \int \rho(r)^{4/3}dr. \tag{2.19}$$

C_x constant is equal to 0.7386. Parametrization of the results of a set of quantum Monte Carlo calculations gives the correlation energy term, $E_c[\rho]$. However, since the electron densities vary in a molecule, it cannot be uniformly distributed. Thus, LDA is not suitable for determination of the exact exchange-correlation functional.

Due to LDA's inadequacy on this issue, Generalized Gradient Approximation (GGA) [34] method is developed. GGA considers the electron density as nonhomogeneous as exchange and correlation energies to depend on density gradient

$$E_{XC}^{GGA}[n] = \int drn(r)\epsilon_{XC}(n(r), |\nabla n(r)|). \tag{2.20}$$

Hybrid density functional methods are alternative approaches that combine GGA with a percentage of Hartree-Fock (HF) exchange. M06-2X [35] is one of the most well-known hybrid functionals that is a member of the Minnesota Functional family. It is based on meta-GGA approximations. Zhao states that M06-2X functional enhances the calculation of atomization energies, ionization potentials, electron, and proton affinities as well as improving the calculation of alkyl-bond dissociation energies, proton affinities of conjugates π systems, binding energies of Lewis acid-base complexes, and heavy atom transfer barrier heights [35, 36]. The hybrid-change correlation can be written as

$$E_{XC}^{hyb} = \frac{X}{100}E_X^{HF} + (1 - \frac{X}{100})E_X^{DFT} + E_C^{DFT} \tag{2.21}$$

where X represents the percentage of Hartree-Fock exchange, and it equals to 54 in M06-2X functional. Another alternative approach is Long-range corrected (LC) [37] hybrid density functionals that have 100% HF exchange for long-range electron-electron interactions. ωB97XD [38] is one of the long-range hybrid functional. It applies a small fraction of short-range exact exchange. The long-range correction advances long-chain polarizability, optical properties, charge-transfer excitations, and dissociation of two-centered three electrons bonds.

The long-range corrected hybrid of a density functional theory approximation (LCDFA) is

$$E_{XC}^{LCDFA} = E_X^{SR-DFA}(\omega) + E_X^{LR-HF}(\omega) + E_C^{DFA}. \tag{2.22}$$

2.3. Basis Sets

Basis set [39] is a set of functions that is used to describe the orbitals in a system. Basis functions are expanded as lineer combinations of atomic orbitals (LCAO) with different coefficients.

$$\phi_i = \sum_{\mu=1}^{K} c_{\mu i} f_\mu \tag{2.23}$$

where μ_i represents molecular orbitals, f_μ atomic orbitals, $c_{\mu i}$ coefficients and K is the total number of atomic orbital functions that are basis functions.

Basis sets are divided into two groups Slater Type Orbitals (STOs) and Gaussian Type Orbitals (GTOs). STOs give an accurate solution for Schrödinger's equation for hydrogen atoms; however, the computational cost is high since a large number of required integrals increase the time required for the computation. GTOs are approximated analogues of STOs.

All orbitals are considered to have the same shape in a minimal basis set and one basis function represents each atomic orbital within an atom. However, it is not realistic to accept all orbitals to have the same shape. Thus, double and triple zeta basis sets have been developed. This time, the computational cost is high when the molecules get bigger since the calculation of double zeta for each orbital becomes costly. To overcome this issue, Pople developed split-valence basis sets. In this method, the core and valence orbitals are treated separately.

Since valence electrons are more affected by the chemical environment than the core electrons, minimal basis function is used for core orbitals and larger basis functions for valence orbitals. The notation of the split-valence basis sets is based on A-BCd. [40] In this notation, A represents the number of primitives for inner shell orbitals, B and C represents the valence orbitals composed of two basis functions for each. The number two after the hyphen (B and C) means that this basis set is a split-valence double zeta basis set.

There are two modification functions to add in basis sets to have better approximations for electronic energy: polarization and diffusion functions. The first one, polarization function is required since the orbitals may have more than one type of angular momentum as they polarize each other when they are mixed. An asterisk (*) at the end of a basis set or (d) implies polarization function is added for heavy atoms while double asterisk ** or (d,p) is used for heavy atoms like hydrogen or helium. The second one, diffuse function, is used for larger orbital occupancies. Anions and electronegative atoms require diffuse function as they have higher electron density. The one plus sign, +, represents the diffuse function that is added to p orbitals while ++ implies it is added to s orbitals.

Schrödinger's equation gets more accurate when the basis sets are more complex. On the other hand, accurate calculations make the computational cost increase. Hence, the selection of basis sets and functionals should depend on the required accuracy level and acceptable computational cost.

2.4. Continuum Solvation Models

Solvation models elucidate the behavior of the solvated condensed phase as they provide a solvent environment. They are needed for more realistic calculations. Two general types are implicit and explicit models. In explicit models, certain numbers of solvent molecules are explicitly added to the model.

In contrast, the implicit -also continuum solvation- model represents the solvent continuum. It considers several physical effects to contribute overall solvation process. The total solvation free energy can be described as

$$\Delta G_{solvation} = \Delta G_{cavity} + \Delta G_{dispersion} + \Delta G_{electrostatic} + \Delta G_{repulsion} \tag{2.24}$$

where ΔG_{cavity} represents the energy of solute addition to the system, $\Delta G_{dispersion}$ implies dispersion interactions between solute and solvent, that stabilizes the system. $\Delta G_{electostatic}$ is the electrostatic interaction energy between solute and solvent and lastly, $\Delta G_{repulsion}$ is the exchange solute-solvent interactions that are not included in the energy of cavitation.

The Polarizable Continuum Model (PCM) [41] is one of the polarizable continuum solvation models. It places the solute in a cavity defined by a set of spheres centered on atoms, having radii defined by the van der Waals radius of the atoms multiplied by a predefined factor. The polarization charges are placed into small domains that the cavity surface is divided into. Mainly, there are three different approaches to perform PCM calculations. The first method is the Dielectric PCM (D-PCM). The second model is the Conductor-like PCM (C-PCM) that the surrounding medium is modeled as a conductor instead of a dielectric. The last one, Integral Equation Formalism of PCM (IEF-PCM) is an implementation at the PCM equations that are reformed.

2.5. The Activation Strain-Distortion/Interaction Model

The activation strain model or distortion/interaction model [42–44] is used to determine the favorable interactions and unfavorable distortions of the reactions. It provides a broad understanding of the physical factors that affect the height of the activation barrier and reactivity patterns when substituents or reactants are changed. The distortion/interaction model contributes to analyzing equilibrium structures, transition states (TS), and nonstationary points of the reaction coordinate.

In this model, the activation energy of a reaction is divided into two contributors

$$\Delta E_0^{\ddagger} = \Delta E_{dist}^{\ddagger} + \Delta E_{int}^{\ddagger} \tag{2.25}$$

where distortion energy ($\Delta E_{dist}^{\ddagger}$) is caused by the structural distortion of reactants and interaction energy ($\Delta E_{int}^{\ddagger}$) stems from the interaction of these distorted reactants. The reaction strain energy ($\Delta E_{dist}^{\ddagger}$) is the required energy to distort the reactants from their equilibrium structures to TS structures. It is determined by rigidity of the reactants [45] and the interaction energy ($\Delta E_{int}^{\ddagger}$) among the reactants depends on their electronic structure and how they are positioned relative to each other during the reaction. In most cases, strain energy has a positive value and is a destabilizing effect, while interaction energy has a negative value and is a stabilizing effect.

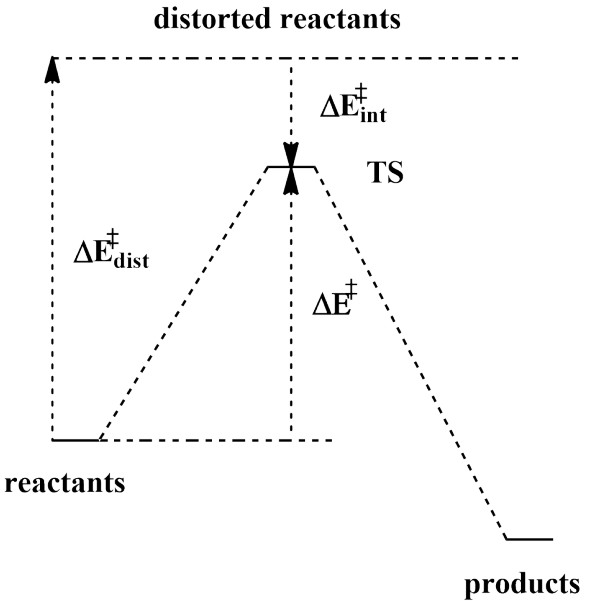

Figure 2.1. Schematic representation of Distortion/Interaction Model

2.6. Noncovalent Interactions

The Noncovalent Interaction(NCI) analysis provides an NCI index that identifies the noncovalent interactions based on the electron density and its derivatives. This index is based on a 2D plot of the reduced density gradient, s, and the electron density, ρ,to visualize the interactions in the low density system as follows

$$s = \frac{1}{2(3\pi^2)^{1/3}} \frac{|\nabla\rho|}{\rho^{4/3}}. \tag{2.26}$$

NCI index contributes to identify and classify the NCIs and NCI plots provide graphical representations of overlapped electron densities of interacting molecules. Accumulation of the density is related to the strength of the interaction.

2.7. Population Analysis and Atomic Charges

There is no quantum mechanical observable for charges of atoms in a molecular system which leads to a lack of original definition for quantum charges. Population analysis methods are used for assigning charges on atoms. The partial atomic charge of a positively charged atomic center Z_A covered with electron density is defined as [46]

$$q_A = Z_A - \int \rho_A(r) dr \tag{2.27}$$

where q_A represents the atomic charge, and Z_A is the charge on nucleus for an atom A. The second term of the Equation 2.27 is the total number of electrons in the system (N) and can be described as

$$N = \sum_{\mu}^{AO} (PS)\mu\mu. \tag{2.28}$$

P represents the electron density and S is the overlap population. Mulliken population analysis [47] is expressed as

$$q_A = Z_A - \sum_{\mu \epsilon A}^{AO} (PS)\mu\mu \tag{2.29}$$

where all of the electronic charges comes from the atomic orbitals that are summed up, electronic overlap population between two atoms are divided between atomic orbitals (AO) which contribute to the corresponding overlap. Mulliken population analysis has a limitation since it is basis function dependent. It assumes that basis functions are centered on nuclei. Being sensitive to basis set size makes the comparison at a different level of theories meaningless.

In addition, this population analysis may result in populations less than 0 or higher than 2. Löwdin analysis [48], less sensitive to basis functions, was developed as an improvement to Mulliken analysis to overcome these negative populations using a nonorthogonal basis.

Another method is Natural Population Analysis (NPA) [49] which provides another perspective than Mulliken and Löwdin. This method is based on the Natural Bond Orbitals (NBO) scheme that distinguishes the electrons that participate in covalent bonds and lone pair electrons. The atomic orbitals are partitioned to the core, valence, and Rydberg orbitals to provide accurate Lewis structure. The partials charges are acquired by summing over Natural Atomic Orbitals (NAO). NPA offers various advantages compared to Mulliken or other alternative approaches. They display numerical stability in the case of changing basis sets when compared with associated energy changes. Besides, NPA defines charge distributions in ionic compounds better where Mulliken populations differ in density integration and empirical measures of ionicity.

2.8. Conceptual DFT

Conceptual DFT developed by Parr [50] is a subfield of DFT that is derived from concepts and principles related to electron density, and it attemps to understand and predict the chemical behavior of a molecule. [51] Parr and co-workers and then theoretical chemists managed to precisely define chemical concepts which are already been known and used, such as electronegativity. It provides contribution to the qualitative knowledge and quantitative prediction of reactivity in chemical terms. Conceptual DFT originally based on the fact that the ground state energy of an N electron system is considered to be dependent on the number of electrons N and the external potential v(r) determined by density as stated in the Hohenberg-Kohn theorem

$$E[\rho(r)] = E[N; v(r)]. \tag{2.30}$$

The system responds to the change of electrons, external potential, or both that contributes to the prediction of the reactivity. The $E[N; v(r)]$ derivatives compose the first series of reactivity indicators, the electronic chemical potential μ, electronegativity χ, chemical hardness η, the Fukui function $f(r)$ and the two variables linear response function χ(r,r'). The electrophilicity index ω is

$$\omega = \frac{\mu^2}{2\eta} \tag{2.31}$$

where μ is electronic chemical potential and η is absolute hardness. The electrophilicity index ω measures the stabilization of energy of a molecule as it accepts electron density. Relative nucleophilicity index (N) relies on the idea that molecules having high nucleophilicity have the lowest ionization potential and it is defined as [52]

$$N = E_{HOMO(Nu)}(eV) - E_{HOMO(TCE)}(eV) \tag{2.32}$$

and based on HOMO energies obtained from Kohn-Sham schemes [53].

2.8.1. Reactivity Descriptors

Reactivity indices are used to characterize the nucleophilic and electrophilic behaviors of molecules in the conceptual DFT framework. The Fukui function $f(r)$ [54] describe the changes in electron density at a point r regarding the variation of the number of electrons N at a fixed external potential $v(r)$ and defined as

$$f(r) = \left(\frac{\partial \rho(r)}{\partial N}\right)_{v(r)}. \tag{2.33}$$

Parr and Yang stated that the reagent approaches the molecule where the chemical potential of the molecule is at maximum value and direction is preferred where the fukui function is largest

$$f^{-}(r) \approx \rho_{HOMO}(r) \tag{2.34}$$

$$f^{+}(r) \approx \rho_{LUMO}(r) \tag{2.35}$$

where $f^{-}(r)$ for electrophilic and $f^{+}(r)$ for nucleophilic attacks. The fukui functions based on Mulliken gross charges $q(r)$are defined [55] as

$$f^{-} = q_k(N) - q_k(N-1) \tag{2.36}$$

$$f^{+} = q_k(N+1) - q_k(N) \tag{2.37}$$

where $q_k(N)$, $q_k(N+1)$, $q_k(N-1)$ are the atomic charges in the neutral, cationic and anionic species. Fukui functions contribute to the characterization of local reactivity of the molecule as they allow dispersion of the global reactivity indices for instance nucleophilicity and electrophilicity indices along the molecule.

The local electrophilicity and nucleophilicity are defined as

$$\omega_k = \omega f_k^+ \tag{2.38}$$

$$N_k = N f_k^- \ . \tag{2.39}$$

Parr functions ${P_k}^+$, ${P_k}^-$ [56, 57] relies on the atomic spin density (ASD) distribution at the radical anion and at the radical cation of a neutral molecule respectively. They identify the most electrophilic and nucleophilic centres of molecules. The Parr functions are described as

$$P^-(r) = \rho_s^{rc}(r) \tag{2.40}$$

$$P^+(r) = \rho_s^{ra}(r) \tag{2.41}$$

where $\rho_s^{rc}(r)$ is the ASD of radical cation and $\rho_s^{ra}(r)$ is the ASD of radical anion.

${P_k}^+$ and ${P_k}^-$ represent electrophilic and nucleophilic Parr functions, respectively. With the help of Parr functions the local electrophilicity [58] and nucleophilicity [59] can be redefined respectively as

$$\omega_k = \omega P_k^+ \tag{2.42}$$

$$N_k = N P_k^- \ . \tag{2.43}$$

Consequently, the most electrophilic (ω_{max}) and nucleophilic (N_{max}) center of the molecule can be identified with the reactivity descriptors.

3. RESULTS

3.1. Computational Procedure

An extensive Density Functional Theory (DFT) study was conducted where KI formation reactions were modeled. The optimizationswere performed at M062X [35,60] level of theory, 6-31+G(d,p) basis set was employed for all atoms except sulfur for which the 6-311++G(3df,3pd) extra basis set was used for higher accuracy [61, 62]. A detailed analysis of possible conformers of all reactants, transition states, and products were performed. M06-2X was selected for its well-known performance in functional organic systems with dispersion effects [63, 64]. All calculations were performed with Gaussian 16 [65] software package. All free energy values are relative to corresponding separate reactants and are reported at 298 K and 1 atm. ΔG_{rxn} for formation reactions of α-halo enamine, ketenimine, ynamine, ynamide and the last step of Ghosez's mechanism are calculated with respect to product complex. Normal mode analysis was performed, as well as Intrinsic Reaction Coordinate (IRC) calculations to verify transition state geometries. [66, 67] The effect of the solvent environment was modeled by means of the self-consistent reaction field (SCRF) theory [68]. Geometry optimizations were performed in chloroform ($CHCl_3$, ε=4.7113), diethyl ether ($(C_2H_5)_2O$, ε=4.2400), and dichloromethane (CH_2Cl_2, ε=8.93) taking into account the experimental conditions of different mechanisms. Specifically, for all calculations performed on Ghosez's mechanism, all compounds are modeled in $CHCl_3$ except for 7a and 10a which are modeled in CH_2Cl_2. Energy refinements were performed with range-separated ω97XD39 [38], double hybrid B2PLYP [69], and hybrid-GGA MPW1K41 [70] functionals and 6-31+G(d,p) basis set. The performance of the functionals on the barrier heights were comparatively analyzed. Natural Population Analysis (NPA) [49] was conducted with the 6-31+G(d,p) basis set. NBO atomic spin density (ASD) was performed with the UM062X/6-311+G(d,p)//M062X/6-311+G(d,p) and Fukui indices were performed with M062X/DZP)//M062X/6-31+G(d,p) to examine KI reactivity.

3.2. Keteniminium Salt Formation: Mechanistic Aspects

A comprehensive DFT study was conducted to explain mechanistic details of four different KI formation reactions. These are the formation reactions of KI from α-halo enamines, ketenimines, ynamines, ynamides, and lastly from Ghosez's reaction (from tertiary amides). Each formation reaction was described in the following sections.

3.2.1. Formation of Keteniminium Salts from α-halo Enamines

The reaction between $ZnCl_2$ and *N,N*-dimethyl-1-chloro-2-methylpropenylamine was modeled in dichloromethane (CH_2Cl_2). Figure 3.1 describes the generation of the KI through simultaneous C-Cl bond breakage and new Zn-Cl bond formation. Hybridization of the central carbon atom changes from sp^2 to sp resulting in a formation of the corresponding KI. Results disclose that the reaction is exergonic and proceeds via a concerted mechanism. Besides, the low activation barrier ($\Delta G^{\ddagger}$= 5.7 kcal.mol^{-1}) in Figure 3.1 indicates that keteniminum salts are readily generated from *N,N*-dimethyl-1-chloro-2-methylpropenylamine in the presence of the Lewis acid $ZnCl_2$.

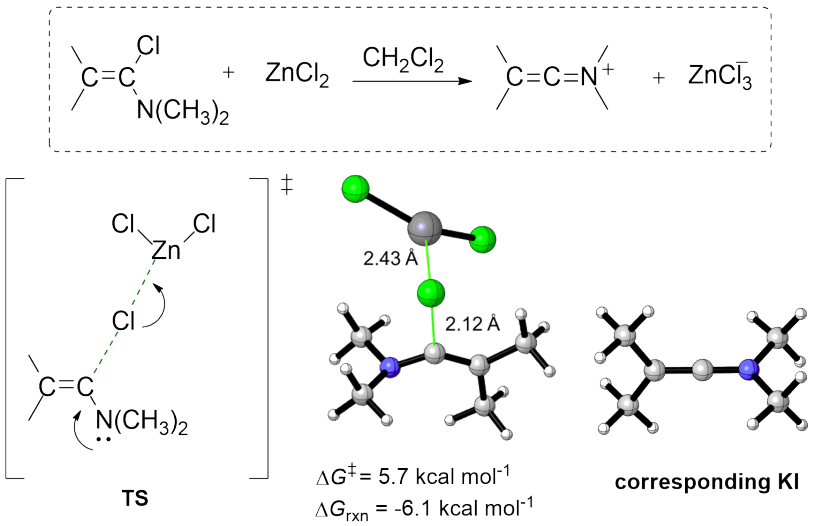

Figure 3.1. Reaction mechanism (M06-2X/6-31+G(d,p)) for the formation of KI salt from α-halo enamines in CH_2Cl_2.

Even though this is a straightforward reaction to generate KI, it is not preferred anymore since it requires the isolation and purification of the α-chloroeneamine and it uses a toxic gas, phosgene, to obtain starting material, enamine. Besides, it is not applicable to synthesize aldo-keteniminium salts [2, 3, 22].

3.2.2. Formation of Keteniminium Salt from Keteniminies

Secondly, alkylation of *N*-(2-tert-butyl-3,3-dimethylbut-1-enylidene) ethanamine by methyl fluorosulfonate (FSO_2OCH_3) was modeled in diethyl ether. The formation reaction takes place *via* an S_N2-type concerted mechanism where the new bond between N_1 and CH_3 forms as ketenimine attacks the methyl and FSO_2O^- leaves simultaneously (Figure 3.2). The direct methylation of the keteneimine by methyl fluorosulfonate is exothermic and has a free energy of reaction ΔG_{rxn}= -12.0 kcal.mol^{-1}. Although direct methylation of ketenimine seems to be an effortless mechanism for the formation of the corresponding KI, its synthetic application is too restricted to be used extensively. [6]

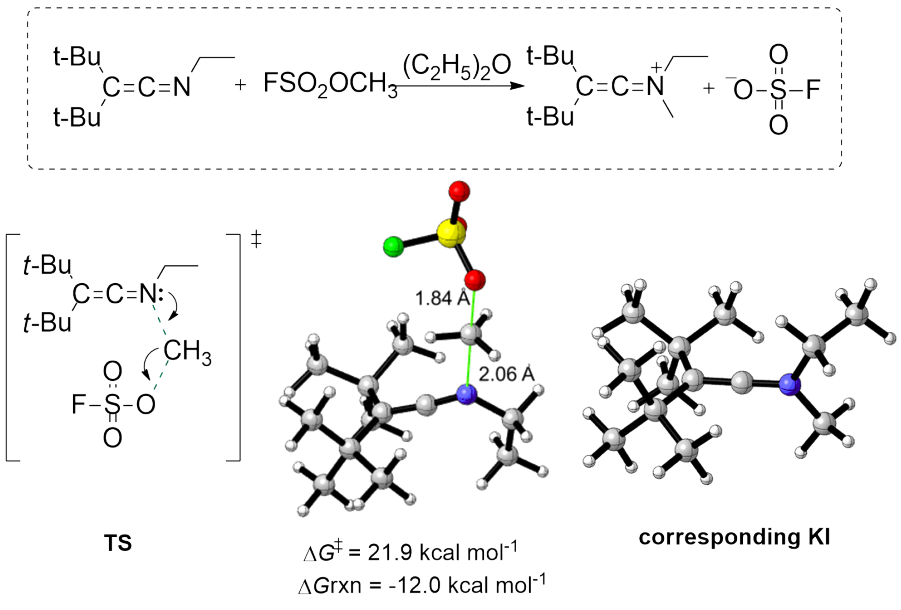

Figure 3.2. Reaction mechanism (M06-2X/6-31+G(d,p)) for the formation of KI salt from ketenimines in $(C_2H_5)_2O$.

3.2.3. Formation of Keteniminium Salts from Ynamines and Ynamides

The reaction between HCl and ynamine **(a)** and ynamide **(b)** were modeled in CH_2Cl_2. DFT results depict that the formation of KI from ynamine has a lower free activation energy and is an exergonic reaction, while generation from ynamide has a higher activation energy and is an endergonic process as reported in Figure 3.3. Being sensitive toward hydrolysis restricts the use of ynamines although the energetics for the formation of KI is more favorable and the corresponding ynamides have found much broader synthetic applications. [1]

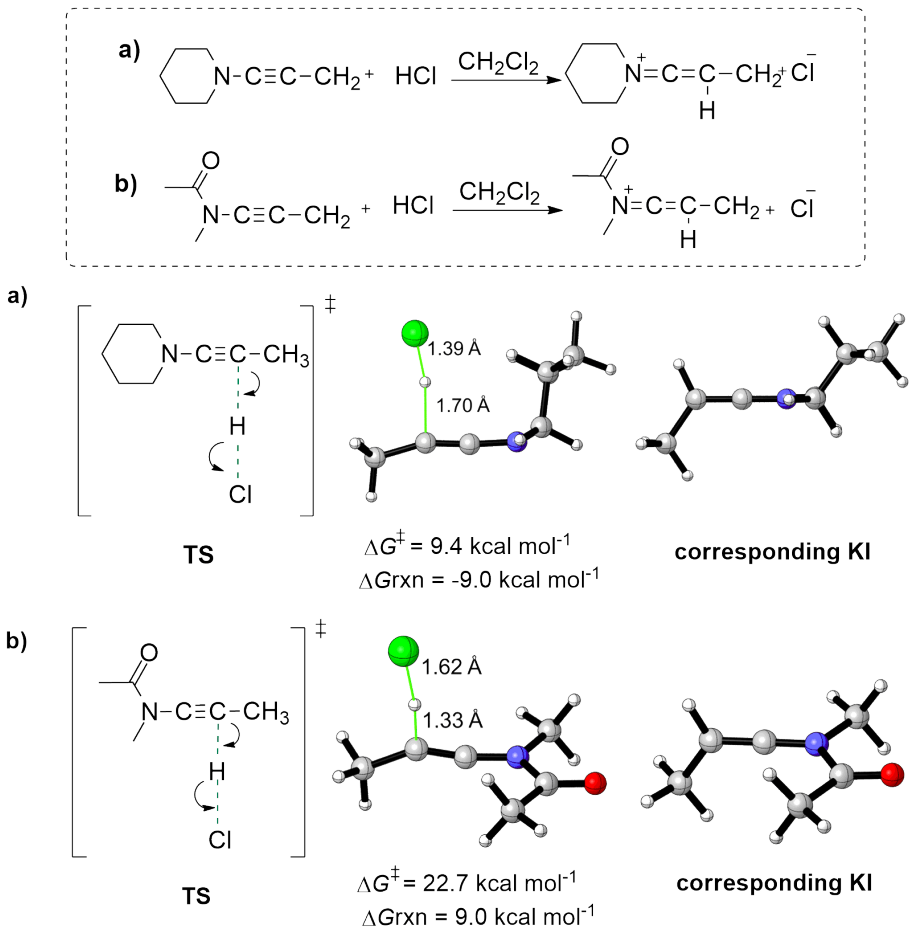

Figure 3.3. Reaction mechanism (MPW1K/6-31+G(d,p)) for the KI formation from a) ynamines and b) ynamides in CH_2Cl_2.

3.2.4. Formation of Keteniminium Salts Through Ghosez's Mechanism

Finally, the mechanism of KI formation from tertiary amides with triflic anhydride and collidine was examined. Piperidine was selected as the N-substituent to provide a better comparison with several experimentally accessible KIs [16, 18, 19, 71–74] as shown in Figure 3.5. Furthermore, the original mechanism with dimethyl substituted nitrogen was also modeled in chloroform and in gas phase (Table 3.1). The energetic results and rate determining step (RDS) are consistent with the piperidine bearing amide. (Figure 3.4).

The first step is the electrophilic activation of starting amide by triflic anhydride. A new bond formation occurs between the amide carbonyl oxygen and sulfur of Tf_2O as the starting amide attacks triflic anhydride and the bond between sulfur and oxygen of triflic anhydride is broken simultaneously (G-TS1 in Figure 3.5). Thus, step one has proven to be concerted. The second step includes hydrogen abstraction from *O*-triflyliminium by collidine, resulting in the formation of α-trifloylenamine. A double bond formation occurs between C_2 and C_3 as the proton is abstracted by collidine. In the last step, the desired keteniminium triflate salt is generated through cleavage of the carbon-oxygen bond of α-trifloylenamine. Computed data show that the first step is the RDS ($\Delta G^{\ddagger}$)= 29.8 kcal.mol^{-1} since it has the highest activation barrier compared to the hydrogen abstraction and the formation of KI steps. The result indicates that the overall KI salt formation process is directly affected by the reactivity of the starting amide towards Tf_2O. *N*-sulfonylated minor product is obtained during electrophilic activation of the amide by triflic anhydride as previously stated by Ghosez and coworkers. [5] Figure 3.6 depicts the formation of this side product. Comparison of the activation barriers of *N*- and *O*-acylated products indicates that the activation barrier of the side reaction ($\Delta G^{\ddagger}$= 27.9 kcal.mol^{-1}) is slightly lower than the major product ($\Delta G^{\ddagger}$= 29.8 kcal.mol^{-1}).

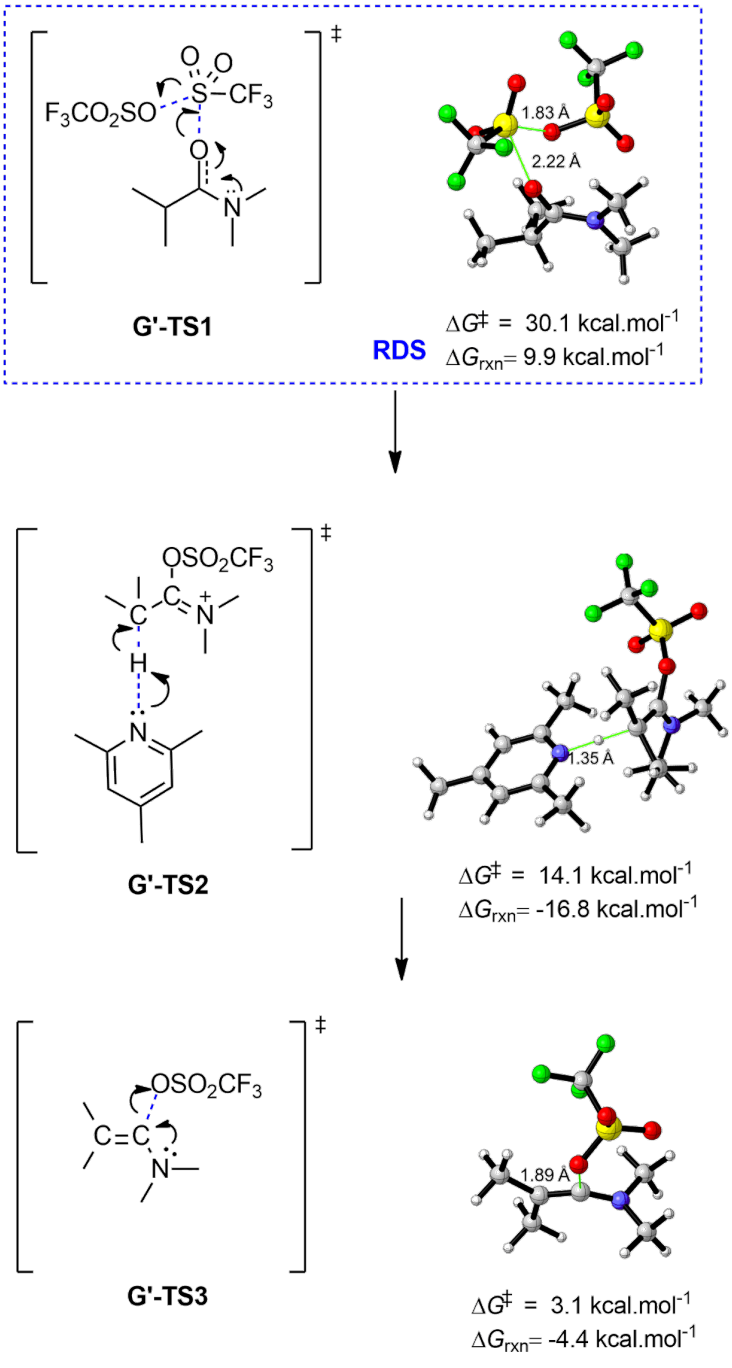

Figure 3.4. Reaction mechanism (M06-2X/6-31+G(d,p)) for Ghosez's reaction [5] with dimethyl substituent in $CHCl_3$.

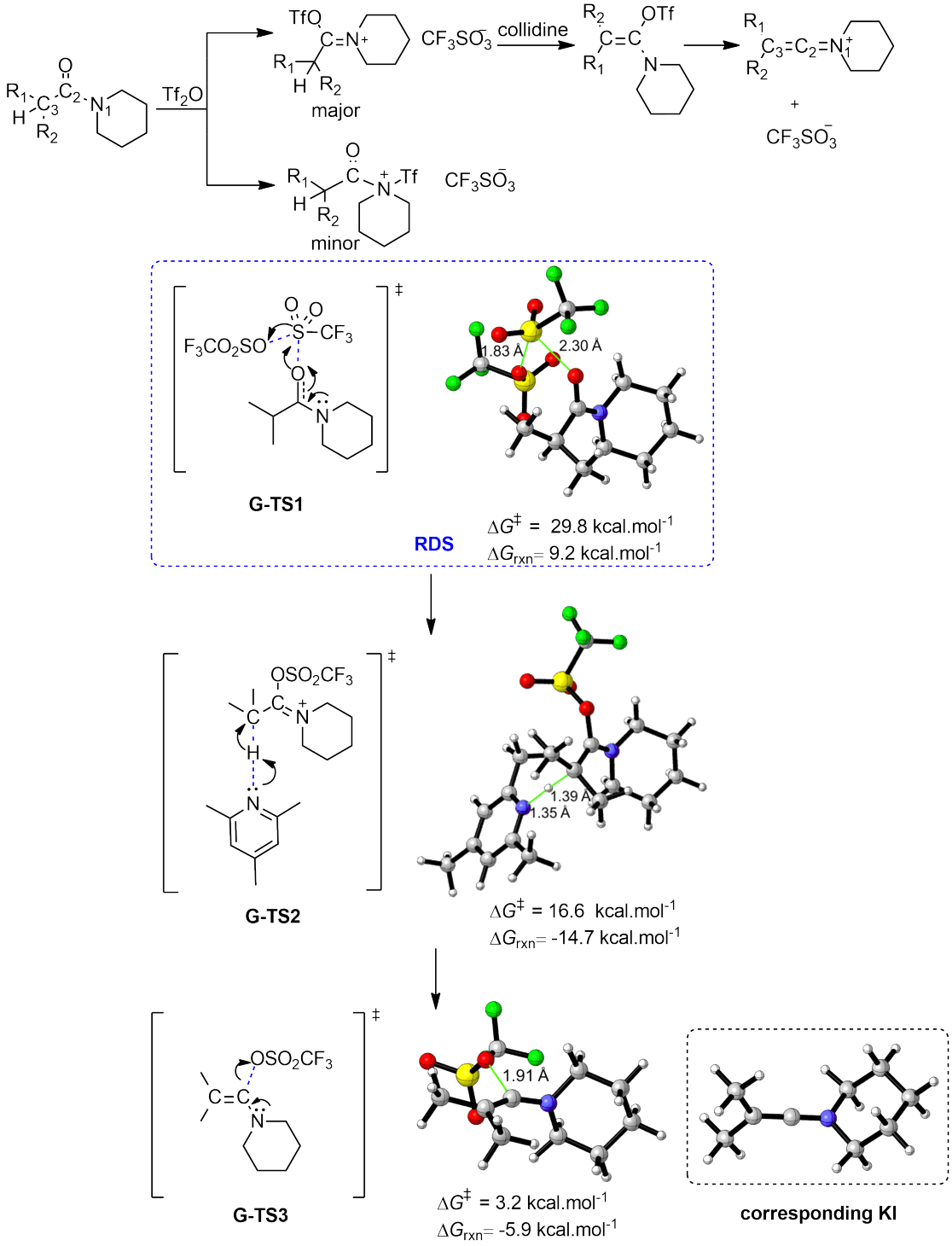

Figure 3.5. Reaction mechanism (M06-2X/6-31+G(d,p)) for Ghosez's reaction [5] in $CHCl_3$.

On the other hand, the KI is a thermodynamically more stable product in comparison to the *N*-sulfonylated side product (ΔG_{rxn}= 24.7 kcal.mol^{-1}). Free energy of activation ($\Delta G^{\ddagger}$) and reaction (ΔG_{rxn}) values are given in Figure 3.6. Side reaction was also modeled for the *N, N*-substituted amide Figure 3.7. All energies are calculated compared to separate reactants. ΔG_{rxn} calculated according to product complex.

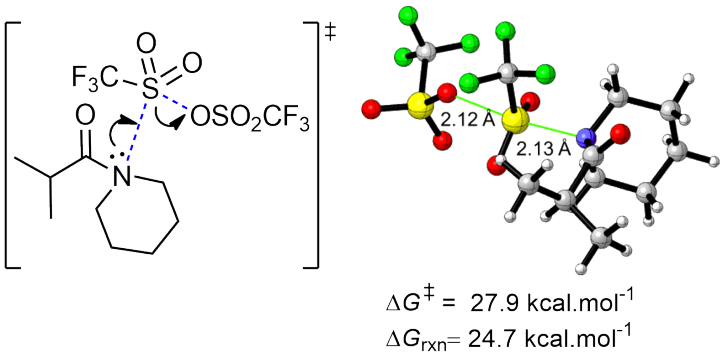

Figure 3.6. Side reaction mechanism (M06-2X/6-31+G(d,p)) for Ghosez's reaction in $CHCl_3$)

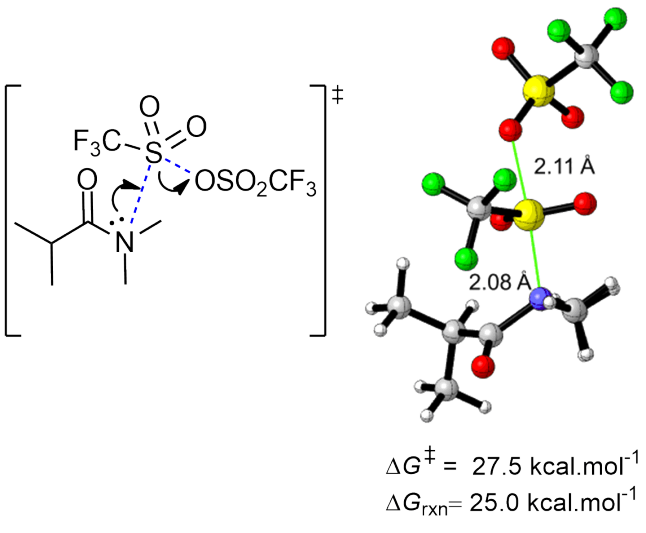

Figure 3.7. Side reaction mechanism (M06-2X/6-31+G(d,p)) for Ghosez's reaction for *N,N*-dimethyl substitutent in $CHCl_3$)

As mentioned previously, the original Ghosez's mechanism was also modeled in a vacuum. The results are depicted in Table 3.1 where all free energies were calculated from complex reactants and products due to presence of ions to avoid BSSE errors. Results gave similar trend with reaction in chloroform as triflation of amide is the rate determining step.

Table 3.1. Gibbs free energy barriers ($\Delta G^{\ddagger}$) and reaction free energies (ΔG_{rxn}) for Ghosez mechanism with dimethyl substituted nitrogen in vacuum

	M06-2X		ωB97XD		MPW1K		B2PLYP	
Entry	$\Delta G^{\ddagger}$	$\Delta \boldsymbol{G}_{rxn}$	$\Delta G^{\ddagger}$	ΔG_{rxn}	$\Delta G^{\ddagger}$	ΔG_{rxn}	$\Delta G^{\ddagger}$	ΔG_{rxn}
1st Step	26.4	1.2	27.2	2.1	30.9	3.5	35.3	4.2
2nd Step	12.8	-10.3	12.0	-10.7	10.6	-12.3	15.7	-12.4
3rd Step	14.7	11.0	12.4	9.6	14.4	12	10.2	5.2

Energy refinements at ω97XD, B2PLYP, and MPW1K levels of theory were conducted in addition to the M06-2X calculations for all mechanisms and tabluated in (Table 3.2). Calculations generally gave similar results.

Consequently, KI formation reactions were examined through four different mechanisms as from α-haloenamines, ketenimines, ynamines, ynamides, and tertiary amides. Since the amide triflation reaction (mentioned as Ghosez's reaction) has milder conditions compared to other three and is the synthetically most used method, the mechanism of it was fully elaborated and the substituent effect on KI formation is investigated on Ghosez's mechanism. The following part of the study includes the energetic analysis of KI formation from Ghosez's mechanism through the effect of different substituents on the starting amides taking into account energetic, steric, and electronic effects. In addition, natural population analysis of amides, distortion/interaction energy analysis, and non-covalent interactions (NCIs) were examined.

Table 3.2. Gibbs free energy of activation ($\Delta G^{\ddagger}$) and reaction free energies (ΔG_{rxn}) for four different keteniminum formation mechanisms with various functionals.

		M06-2X		ωB97XD		MPW1K		B2PLYP	
	Entry	$\Delta G^{\ddagger}$	ΔG_{rxn}	$\Delta G^{\ddagger}$	ΔG_{rxn}	$\Delta G^{\ddagger}$	ΔG_{rxn}	$\Delta G^{\ddagger}$	ΔG_{rxn}
1	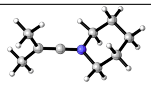 tertiary amide	3.9	-5.3	1.7	-7.0	3.5	-4.5	0.4	-11.4
2	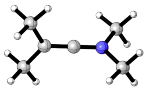 α-enamine	7.4	-4.2	9.6	-15.7	15.5	5.0	16.4	0.4
3	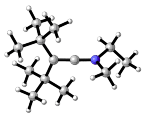 ketenimine	21.9	-12.0	19.7	-18.6	24.7	-7.7	26.2	-6.0
4	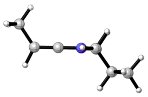 ynamine	3.6	-9.1	2.5	-11.9	9.4	-9.0	5.3	-8.3
5	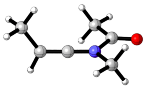 ynamide	10.4	10.4	20.5	6.8	22.7	9.0	25.6	7.5

3.3. The Energetics of KI Formation from Ghosez's Mechanism

After exploring the mechanistic aspects of different KI formation reactions, substituent effect on the amide reactivity was investigated in particular for Ghosez's mechanism. Results showed that KI formation from the reaction of tertiary amides with Tf_2O and collidine has three consecutive steps (Figure 3.1). Electrophilic activation of amide, the first step of the reaction, is the RDS (Figure 3.8). The ease of KI formation and the reactivity of corresponding KI is greatly affected by amide reactivity.

Therefore, experimentally available amides [16, 18, 19, 71–74] were selected and their substituent placement, named C_3 and N_1 substituents (Figure 3.8) were analyzed regarding energetic, electronic, and steric effects.

To verify the RDS with different substituents, second and third steps of Ghosez's mechanism were also investigated along with the firts step. (Tables 3.3 - 3.11 and A.1-A.6). In general, EDG substituted reactants have lower activation barrier in comparison to EWG substituted ones regardless of being in C_3 or N_1 position for RDS of the mechanism.

The substituent effect were discussed for each step to verify the RDS for all steps in the next section and followed by natural population analysis, distortion/interaction energy analysis and non-covalent interactions (NCIs) for amide reactivity.

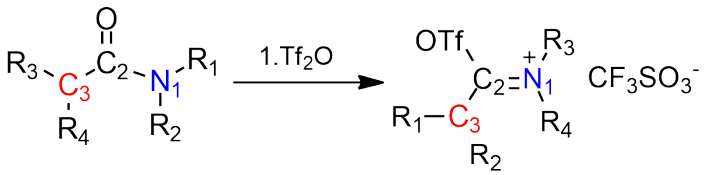

Figure 3.8. First step of Ghosez's mechanism with C_3 and N_1 atoms labeled.

3.3.1. Effect of Substituents on First Step of Ghosez's Mechanism

Amides bearing EDG and EWG substituents generating experimentally available KIs were chosen to investigate the effect of substituents on RDS. The formation and reactivity of KI and tabulated in Table 3.3. Firstly, the effect of C_3 substituents were examined. According to computed data, in general, substituents having the electron-donating ability eases nucleophilic addition reaction of the amide carbonyl oxygen to the strongly electrophilic triflic anhydride by increasing the electron density on oxygen and have similar activation barriers within a range of 2.1 kcal.mol^{-1}, whereas EWGs increase the activation barrier by inductively lowering the electron density on oxygen.

Inductive and steric effects can elucidate the relatively modest effect of C_3 substituents on activation barriers. When EDGs are examined, *N,N*-dimethyl substituted amide 1a ($\Delta G^{\ddagger}$ = 29.8 kcal/mol) has an activation barrier higher than the isopropyl substituted amide 2a ($\Delta G^{\ddagger}$ = 27.9 kcal/mol). The amide bearing dimethyl substituent leads 1.9 kcal.mol^{-1} difference betwen activation energies, which indicates the effect of the sterics around the carbonyl moiety (Figure 3.9).

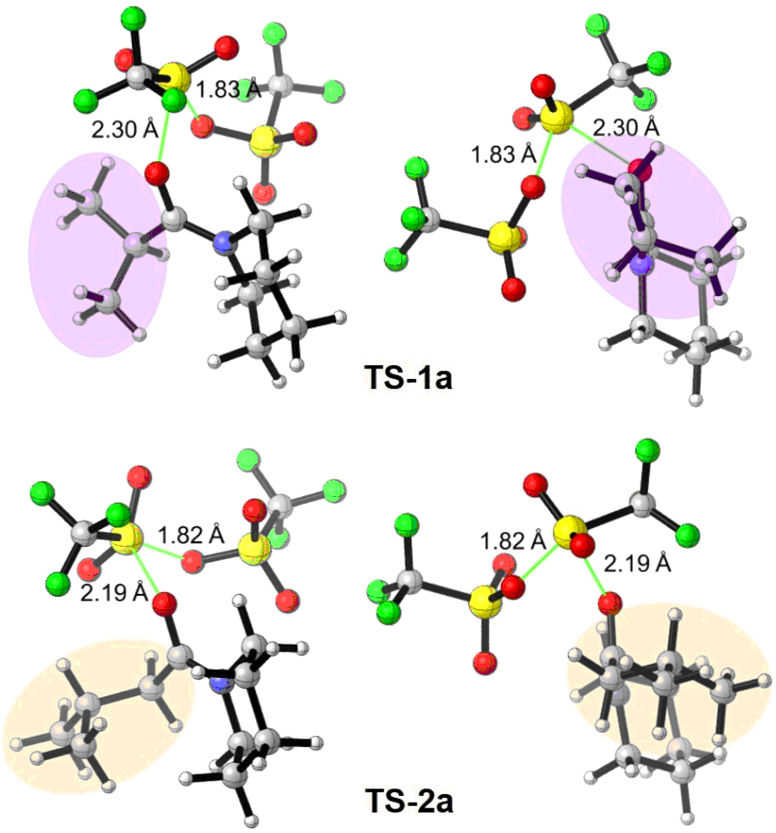

Figure 3.9. Optimized structures of TS-1a and TS-2a. M06-2X/6-31+G(d,p) with IEF-PCM in $CHCl_3$.

In the case of amides with rings, close activation energy values in the range of 27.2 - 28.6 kcal.mol^{-1} were observed in amides bearing aromatic rings adjacent to the carbonyl moiety (3a and 4a) and amides with cyclic rings (5a and 6a). The electron density of the aromatic and of the cyclic [72, 73] rings might contribute to the stabilization of the trifloyliminium ion.

In the case of EWGs, amides 7a, and 8a demonstrate increasing activation barriers due to the inductive effects of the EWGs in the β-position. The highest activation energy among them is observed in 8a ($\Delta G^{\ddagger} = 30.5$ kcal.mol^{-1}) that carries the strongest electron-withdrawing alkyne group even though it is in a smaller size compared to its vinyl 7a analog. Notably, β-trifluoromethyl substituent 10a ($\Delta G^{\ddagger} = 31.3$ kcal.mol^{-1}) has a higher activation barrier than α-chlorine substituent 15a ($\Delta G^{\ddagger} = 29.7$ kcal.mol^{-1}) . The decreased electron density of the carbonyl oxygen of 10a caused by the strong inductive effect of trifluoromethyl substituent leads this energy barrier difference. The highest activation barrier belongs to the phenyl sulfide substituted amide 11a ($\Delta G^{\ddagger} =$ 32.2 kcal.mol^{-1}), that is even higher than the phenyl ether 12a ($\Delta G^{\ddagger} = 30.9$ kcal.mol^{-1}) and the aniline 13a ($\Delta G^{\ddagger} = 30.5$ kcal.mol^{-1}) substituted amides. The higher activation barrier for the phenyl sulfide substituted amide 11a was unexpected, since sulfur has a lower electronegativity compared to oxygen and nitrogen. The longer bond length and the higher bond angle of the C-S bond compared to their oxygen and nitrogen analogs are expected to ease the reaction with Tf_2O. Nevertheless, sulfur and methyl groups created a steric hindrance, which might result in rotational barrier bringing about the increased activation barrier. Figure 3.10 depicts that TS-12a and TS-13a have stabilizing interactions that lowers the activation barriers and TS-11a prefers a less crowded orientation. Further investigation of this situation is discussed in the following sections by means of NCI. The steric hindrance of the methyl- and the X-phenyl groups in 11a-13a adjacent to the amide increases the activation barrier compared to their parent derivatives 16a-18a.

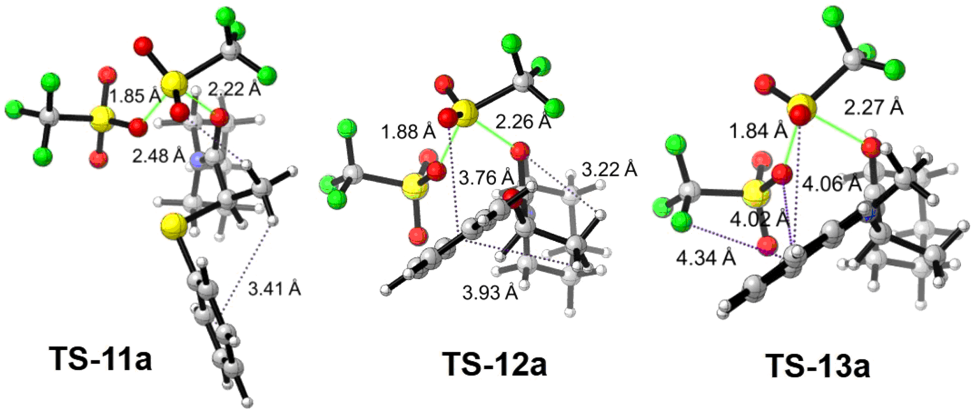

Figure 3.10. Optimized structures of TS-11a, TS-12a and TS-13a. M06-2X/6-31+G(d,p) in $CHCl_3$.

However, parent X-Ph substituted amides, phenyl ether substituted amide 17a ($\Delta G^{\ddagger}$ = 30.1 kcal.mol^{-1}) has the highest barrier among phenyl sulfide 16a ($\Delta G^{\ddagger}$ = 28.7 kcal.mol^{-1}) and aniline 18a ($\Delta G^{\ddagger}$ = 29.5 kcal.mol^{-1}) substituted amides and the expected trend is observed. This difference between parent 16a-18a and methyl-substituted 11a-13a amides stems from the steric hindrance that the methyl group on C_3 caused. Also, formations of 11a-13a supports the formation of 16a-18a considering the energetic results. -SPh, -OPh, and -NRPh substituted amides synthetically provided the corresponding KI leading to high yield benzothiophenes, benzofurans and indoles, respectively [18–21].

A prominent increase in the activation barrier is observed for the trifluoroethyl 10a amide ($\Delta G^{\ddagger}$ = 31.3 kcal.mol^{-1}), in comparison to 2a, which stems from the strong inductive effect of the trifluoromethyl substituent that decreases electron density on the oxygen atom of the amide. Amides 3a and 9a have an aromatic ring and 5a cyclopropyl derivative adjacent to the carbonyl group demonstrates similar activation energies ($\Delta G^{\ddagger}$ = 27.9 kcal.mol^{-1}, $\Delta G^{\ddagger}$ = 27.8 kcal.mol^{-1}, $\Delta G^{\ddagger}$ = 27.7 kcal.mol^{-1}, respectively). The electron density of the aromatic and of the cyclopropyl [72,73] rings might contribute to the stabilization.

Various experimentally available amides were chosen for the investigation of the effect of N_1 substituents on the RDS and, formation and reactivity of KI are tablulated in Table 3.4. The lowest free activation energy belongs to piperidine and *N, N*-dimethyl substituted amides 1a and 1b ($\Delta G^{\ddagger}$ = 29.8 kcal.mol^{-1} and 30.1 kcal.mol^{-1}, respectively) . Electron-donating ability of piperidine and *N, N*-dimethyl groups cause their activation barrier to be lowest among the amides tabulated in Table 3.4. In comparison with the piperidine ring, benzyl 3b ($\Delta G^{\ddagger}$ = 32.1 kcal.mol^{-1}) and diallyl 2b ($\Delta G^{\ddagger}$ = 32.6 kcal.mol^{-1}) substituted amides have higher activation barriers owing to higher steric hindrance and having more sp^2 hybridized carbons than corresponding sp^3hybridized ones that creates an electron withdrawing effect . Cyanomethyl 4b and trifluoroethyl 5b, ($\Delta G^{\ddagger}$ = 33.7 kcal.mol^{-1}) and ($\Delta G^{\ddagger}$ = 33.5 kcal.mol^{-1}) substituted amides have the highest activation barriers. These higher activation barriers can be explained by the presence of strong electron withdrawing groups, trifluoromethyl and nitrile which decrease the electron density on the N_1 atom. Thus, they reduce the reactivity of amide carbonyl oxygen towards triflic anhydride. Consequently, similar EDG and EWG effects were observed with the C_3 substituents.

Furthermore, energy refinements at B2PLYP, MPW1K, and ωB97XD were also performed, and free energies calculated from seperate products for the electrophilic activation of amide are given in Table 3.5 and Table 3.4 Generally, similar barrier trends were displayed regardless of the level of theory. All reported Gibbs free energy values for Ghosez's reaction steps were according to the separate reactants and products except for last step in which reaction free energies were calculated from product complexes. IRC calculations were performed to see the consistency of results for different substituents and tabulated in Table A.1 and Table A.2 which included pre-reactive complex (PRC) and product complex (PC) energy values with the separate reactants, transition states and separate products. Energies of pre-reactive complexes are generally higher than the separate reactants and product complex energies are higher than separate ones due to the presence of TfO^-.

Table 3.3. Free energy barriers ($\Delta G^{\ddagger}$) and reaction free energies (ΔG_{rxn}) for C_3 substituted amides for first step of Ghosez's mechanism.

	Amide	$\Delta G^{\ddagger}$	ΔG_{rxn}		Amide	$\Delta G^{\ddagger}$	ΔG_{rxn}		Amide	$\Delta G^{\ddagger}$	ΔG_{rxn}
1a	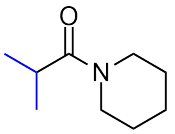	29.8	9.2	**7a**	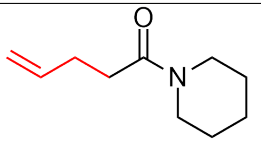	29.6	1.2	**13a**	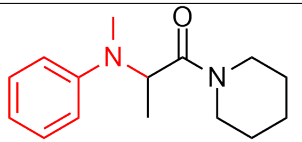	30.5	9.2
2a	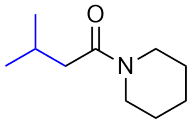	27.9	7.5	**8a**	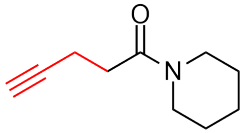	30.5	11.1	**14a**	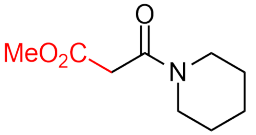	28.5	12.5
3a	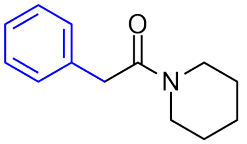	28.0	8.9	**9a**	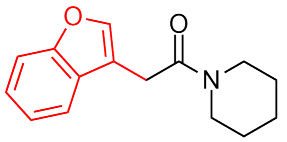	27.8	10.7	**15a**	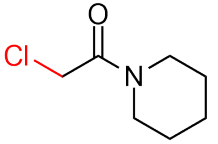	29.7	14.9
4a	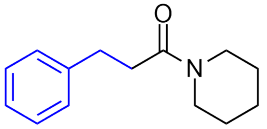	28.6	8.5	**10a**	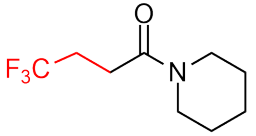	31.3	4.8	**16a**	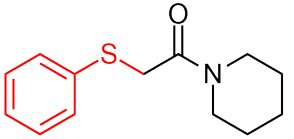	28.8	7.7
5a	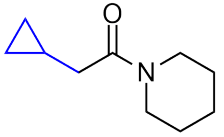	27.7	5.5	**11a**	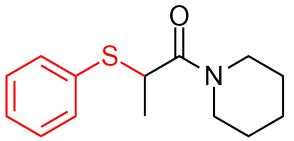	32.2	13.1	**17a**	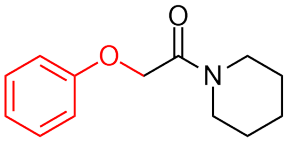	30.1	12.3
6a	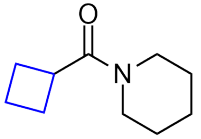	27.9	6.7	**12a**	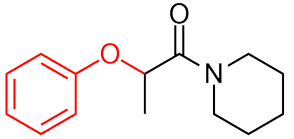	30.9	11.7	**18a**	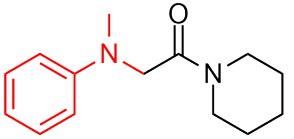	29.5	7.8

Table 3.4. Free energy barriers ($\Delta G^{\ddagger}$) and reaction free energies (ΔG_{rxn}) for N_1 substituted amides for first step of Ghosez's mechanism.

		M06-2X		ωB97XD		MPW1K		B2PLYP	
	Amide	$\Delta G^{\ddagger}$	ΔG_{rxn}	$\Delta \boldsymbol{G}^{\ddagger}$	ΔG_{rxn}	$\Delta G^{\ddagger}$	$\Delta \mathbf{G}_{rxn}$	$\Delta \boldsymbol{G}^{\ddagger}$	$\Delta \mathbf{G}_{rxn}$
1b	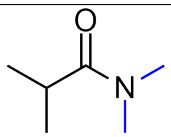	30.1	9.9	30.3	5.6	38.7	7.0	44.5	5.9
1a	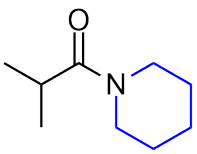	29.8	9.2	32.2	7.3	41.8	9.2	47.3	7.8
2b	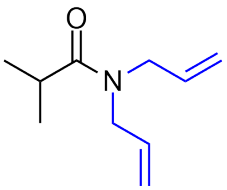	32.6	11.1	35.1	10.3	44.3	12.9	50.4	11.7
3b	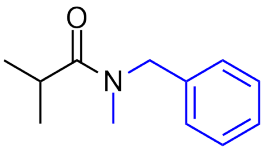	32.1	11.4	35.7	10.1	45.3	13.7	51.3	12.7
4b	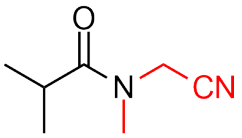	33.5	22.6	36.9	22.1	46.3	24.4	52.0	23.3
5b	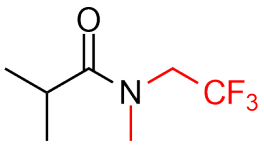	33.7	18.7	36.5	17.3	45.9	19.5	51.6	18.5

The reactivity of starting amides is critical in the formation, since electrophilic activation of the starting amide is the RDS. Computed results are consistent with the increased reactivity of amide as a minimum steric hindrance and higher electron density is present around the carbonyl. Conversely, having an EWGs on N_1 and C_3 atoms increases the activation barrier and reduces the reactivity of amide towards Tf_2O. The following sections include the substituent effect on second and third of Ghosez's mechanism to verify the RDS with different substituents.

Table 3.5. Free energy barriers ($\Delta G^{\ddagger}$) and reaction free energies (ΔG_{rxn}) for C_3 substituted amides with various functionals for the first step of Ghosez's mechanism.

	M06-2X		ωB97XD		MPW1K		B2PLYP	
Entry	$\Delta G^{\ddagger}$	$\Delta \boldsymbol{G}_{rxn}$	$\Delta G^{\ddagger}$	$\Delta \boldsymbol{G}_{rxn}$	$\Delta G^{\ddagger}$	ΔG_{rxn}	$\Delta G^{\ddagger}$	$\Delta \boldsymbol{G}_{rxn}$
1a	29.8	9.2	32.2	7.3	41.8	9.2	47.3	7.8
2a	27.9	9.2	30.0	5.1	39.5	7.9	45.3	6.2
3a	28.0	8.9	30.5	7.0	39.6	10.0	45.4	8.9
4a	28.6	8.5	30.5	6.0	38.8	7.9	44.3	6.4
5a	27.7	5.5	30.1	3.4	37.8	4.8	43.4	3.4
6a	27.9	6.7	31.2	5.3	40.3	7.1	45.8	5.5
7a	29.6	1.2	32.8	-0.3	41.5	0.9	47.0	-1.0
8a	32.2	7.3	30.5	11.1	42.4	10.0	47.9	8.4
9a	27.8	10.7	30.3	8.7	37	9.8	42.3	8.2
10a	31.3	4.8	32.8	1.7	41.7	3.0	47.4	1.4
11a	32.2	13.11	35.6	11.5	44.5	13.1	50.0	11.2
12a	30.9	11.7	34.6	11.3	45.2	13.5	52.1	11.4
13a	30.5	9.2	34.7	8.5	46.0	10.6	51.1	9.4
14a	28.5	12.5	30.8	10.6	38.6	12.5	44.3	11.1
15a	29.7	14.9	32.4	13.5	39.3	14.1	44.8	12.5
16a	28.8	7.7	31.3	5.1	41.8	9.5	47.8	9.1
17a	30.1	12.3	32.5	12.5	38.8	12.8	43.8	10.4
18a	29.5	7.8	33.7	7.4	43	7.6	48.5	5.9

3.3.2. Effect of Substituents on Second Step of Ghosez's Mechanism

After the investigation of first step of the reaction, the second step, the proton abstraction from *O*-triflyliminium by collidine, resulting in the formation of α-trifloylenamine (Figure 3.11) was energetically investigated and tabulated in Table 3.6 and 3.7. Generally, α-trifloylenamines generating aldo KIs have higher activation barriers when bearing EDG C_3 substituents. Since electron donating ability of the substituents destabilizes the conjugate base α-trifloylenamines inductively, stabilization of the triflyliminium increases the activation barrier. Although the EWGs generally have lower activation barriers, since keto triflyliminiums have steric hindrance around the acidic hydrogen to be abstracted, their activation barriers are higher among EWGs. Effect of N_1 substituents were lower compared to C_3 substituents. However, the same trend was observed between EWG and EDG groups. Thus, inductive and steric effects can account for the effect of C_3 substituents on proton abstraction of triflyliminium.

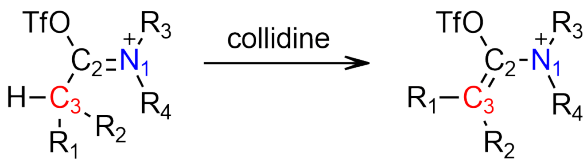

Figure 3.11. Second step of Ghosez's mechanism with C_3 and N_1 atoms labeled.

In the case of EDGs on C_3 atom, isopropyl substituted triflyliminium 2a ($\Delta G^{\ddagger}$ = 18.4 kcal.mol^{-1}) has the higher activation barrier due to its highly electron donating ability, which lowers the acidity of hydrogen adjacent to C_3 by destabilizing its conjugate base. It is followed by the dimethyl 1a ($\Delta G^{\ddagger}$ = 16.6 kcal.mol^{-1}) and cyclobutyl 6a ($\Delta G^{\ddagger}$ = 13.5 kcal.mol^{-1}) substituted ones, which are crowded around the acidic hydrogen relative to other EDGs. Aromatic 4a and cyclic ring 5a bearing triflyliminiums displayed similar activation energies around 11.8/11.9 kcal.mol^{-1}. Phenyl substituted triflyliminium 3a, have the lowest activation barrier ($\Delta G^{\ddagger}$ = 8.3 kcal.mol^{-1}) among EDGs as it has a ring very close to the acidic hydrogen as it hinders the collidine to abstract it.

In the case of EWGs, electron withdrawing ability of the substituent lowers the activation barrier compared to EDGs as conjugate bases of triflyliminiums are stabilized. The significant activation barrier difference between β-positioned EWG substituted α-trifloylenamine 7a ($\Delta G^{\ddagger}$ = 14.8 kcal.mol^{-1}) and 8a ($\Delta G^{\ddagger}$ = 8.7 kcal.mol^{-1}) can be explained with the higher electron drawing ability and smaller size of alkyne. The lowest activation barrier belongs to triflyliminium bearing a methyl acetate group 14a ($\Delta G^{\ddagger}$ = 5.4 kcal.mol^{-1}) on its α-position, which is lower than its α-chlorine analogue 15a ($\Delta G^{\ddagger}$ = 8.3 kcal.mol^{-1}), since it has higher inductive effect. X-phenyl group substituted triflyliminiums 11a-13a showed an unexpected trend as phenyl sulfide have lower activation barrier, even though sulfur is less electronegative than its oxygen 12a ($\Delta G^{\ddagger}$ = 14.0 kcal.mol^{-1}) and nitrogen 13a ($\Delta G^{\ddagger}$ = 15.2 kcal.mol^{-1}) analogues. Similar unexpected trend for these three structures was also observed in first step, and the lower activation barrier of 11a in hydrogen abstraction step may be explained with the same reason with first step as 11a prefers less crowded orientation and the conjugate base would be less stabilized than 12a and 13a. However, the expected trend was observed in their parent analogues 16a-18a. The activation barriers followed the expected order, same as the electronegativity order of phenyl ether 17a ($\Delta G^{\ddagger}$ = 6.0 kcal.mol^{-1}), aniline 18a ($\Delta G^{\ddagger}$ = 9.7 kcal.mol^{-1}), and phenyl sulfide 16a ($\Delta G^{\ddagger}$ = 12.4 kcal.mol^{-1}). Moreover, all these parent structures have relatively lower activation barriers than their analogues with mehtyl group. The additional electron donating methyl group hinders the collidine attack to the acidic hydrogen of triflyliminium.

N_1 substituent effect was also investigated and tabulated in Table 3.7. Generally, the same trend with C_3 substituents were observed as EDGs relatively increase the activation barrier compared to EWGs. Activation barriers of EDGs are similar for piperidine 1a ($\Delta G^{\ddagger}$ = 16.6 kcal.mol^{-1}), diallyl 2b ($\Delta G^{\ddagger}$ = 17.8 kcal.mol^{-1}) and benzyl 3b ($\Delta G^{\ddagger}$ = 7.8 kcal.mol^{-1}) substituted ones in the range of 1.2 kcal.mol^{-1} and higher than dimethyl substituted one 1b ($\Delta G^{\ddagger}$ = 14.1 kcal.mol^{-1}), which have smaller size than the others. β-positioned EWGs 4b ($\Delta G^{\ddagger}$ = 10.2 kcal.mol^{-1}) and 5b ($\Delta G^{\ddagger}$ = 14.2 kcal.mol^{-1}) generally have lower activation barriers compared to EDG substituted ones.

Table 3.6. Free energy barriers ($\Delta G^{\ddagger}$) and reaction free energies (ΔG_{rxn}) for C_3 substituted amides for second step of Ghosez's mechanism.

	KI	$\Delta G^{\ddagger}$	ΔG_{rxn}		KI	$\Delta G^{\ddagger}$	ΔG_{rxn}		KI	$\Delta G^{\ddagger}$	ΔG_{rxn}
1a	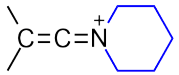	16.6	-1.1	**8a**	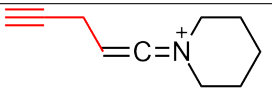	8.7	-11.4	**15a**	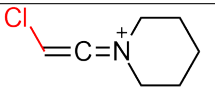	8.3	-15.5
2a	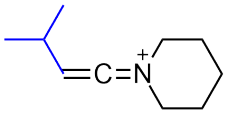	18.4	-10.6	**9a**	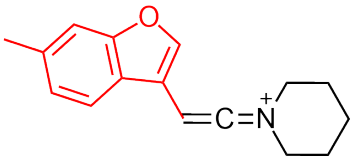	9.4	-14.6	**16a**	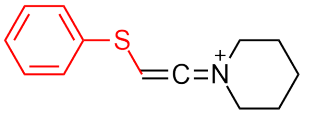	12.4	-11.4
3a	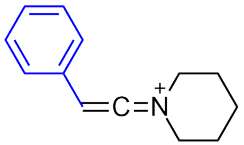	8.3	-14.0	**10a**	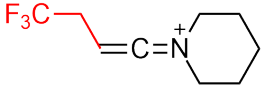	7.0	-12.5	**17a**	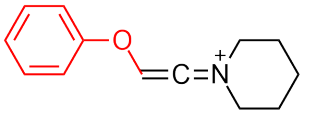	6.0	-14.4
4a	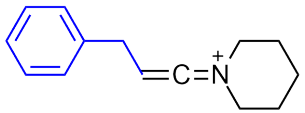	11.8	-10.6	**11a**	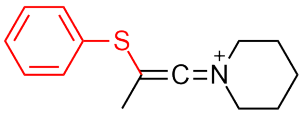	13.7	-11.0	**18a**	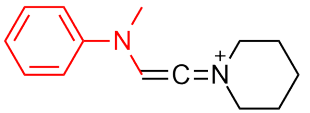	9.7	-12.8
5a	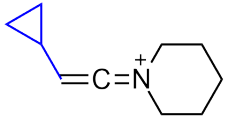	11.9	-9.8	**12a**	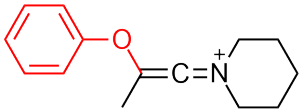	14.0	-5.2				
6a	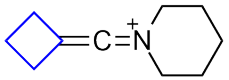	13.5	-10.4	**13a**	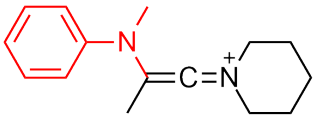	15.2	-18.7				
7a	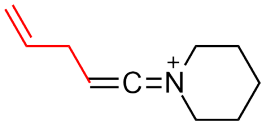	14.8	-6.4	**14a**	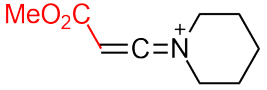	5.4	-18.4				

Table 3.7. Free energy barriers ($\Delta G^{\ddagger}$) and reaction free energies (ΔG_{rxn}) for N_1 substituted amides for second step of Ghosez's mechanism with different functionals.

		M06-2X		ωB97XD		MPW1K		B2PLYP	
	KI	$\Delta G^{\ddagger}$	ΔG_{rxn}	$\Delta G^{\ddagger}$	ΔG_{rxn}	$\Delta G^{\ddagger}$	ΔG_{rxn}	$\Delta G^{\ddagger}$	ΔG_{rxn}
1b	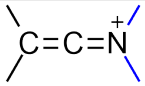	14.1	-16.8	14.1	-15.4	24.1	-15.7	32.5	-15.2
1a	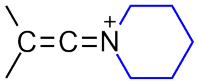	16.6	-15.8	15.1	-15.9	25.4	-17.1	33.8	-16.7
2b	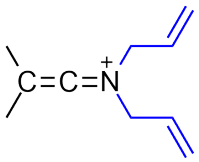	17.8	-17.7	16.4	-18.2	26.4	-19.0	35.1	-18.4
3b	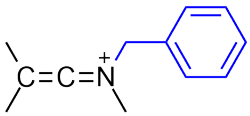	17.8	-16.9	16.3	-17.3	24.5	-19.8	32.6	-19.3
4b	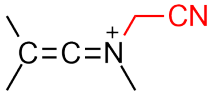	10.2	-28.5	7.6	-29.5	17.3	-31.6	25.3	-31.3
5b	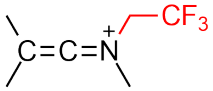	14.2	-23.4	13.0	-23.2	22.6	-24.5	31.0	-25.0

Energy refinements with ωB97XD, B2PLYP, and MPW1K were performed, and free energies of activation and reaction with these functionals were tabulated Table 3.8 and Table 3.7. Similar barrier trends were observed regardless of the level of theory. IRC calculations were also tabulated in Table A.4 and Table A.3.

As a result, electronic and steric effects of substituents are important for the H abstraction step as they determine the acidity of α-trifloylenamine. Generally, EDGs increase the activation barrier as they destabilize the conjugate base and lower the acidity of α-trifloylenamine's alpha H, while EWGs affect reversely. Activation barriers of the second step are lower for all substituents compared to the first step.

Table 3.8. Free energy barriers ($\Delta G^{\ddagger}$) and reaction free energies (ΔG_{rxn}) for C_3 substituted amides for second step of Ghosez's mechanism with different functionals.

	M06-2X		ωB97XD		MPW1K		B2PLYP	
Entry	$\Delta G^{\ddagger}$	ΔG_{rxn}	$\Delta G^{\ddagger}$	ΔG_{rxn}	$\Delta G^{\ddagger}$	ΔG_{rxn}	$\Delta G^{\ddagger}$	ΔG_{rxn}
1a	16.6	-15.8	15.1	-15.9	25.4	-17.1	33.8	-16.7
2a	18.4	-10.6	17.0	13.0	27.7	15.4	35.9	13.7
3a	8.25	-14.0	7.2	-13.3	15.7	-15.9	22.9	-15.5
4a	11.8	-10.6	10.4	-9.4	23.0	-9.5	31.6	-8.5
5a	11.9	-9.8	10.8	-9.4	20.4	-10.7	27.7	-11.3
6a	13.5	-10.4	12.1	-11.0	22.7	-12.4	30.7	-13.1
7a	14.8	-3.3	12.2	-1.2	22.7	-1.1	30.1	-1.2
8a	8.7	-11.4	8.2	-11.3	18.2	-11.4	25.6	-11.8
9a	9.4	-14.6	6.4	-13.1	17.3	-16.3	24.3	-16.2
10a	7.1	-12.5	5.5	-8.3	15.8	-8.6	23.3	-8.0
11a	13.7	-11.0	12.3	-18.7	24.8	-5.3	33.9	-19.0
12a	14.0	-5.2	12.0	-19.4	27.0	-17.8	37.1	-15.9
13a	15.2	-18.7	13.1	-19.0	29.0	-6.3	39.4	-20.8
14a	5.4	-18.4	3.1	-17.7	11.9	-19.8	15.6	-18.8
15a	8.3	-15.5	7.6	-15.2	15.9	-15.4	22.8	-13.8
16a	12.4	-11.4	10.7	-10.2	18.6	-14.1	21.8	-13.5
17a	6.0	-14.4	1.0	-16.4	10.1	-16.7	14.4	-15.3
18a	9.7	-12.8	6.8	-13.6	20.3	0.7	28.5	-13.5

The third step of the Ghosez's reaction was investigated in the next section to determine whether the first step is indeed RDS for all substituents.

3.3.3. Effect of Substituents on Third Step of Ghosez's Mechanism

Finally, the last step of Ghosez's formation reaction, elimination of triflate ion from α-trifloylenamine, was investigated. Free energy barriers ($\Delta G^{\ddagger}$) and reaction free energies (ΔG_{rxn}) of the last step of C_3 and N_1 substituted KIs are tabulated in Tables 3.10 and 3.9. Reaction free energies were calculated according to their product complexes due to the triflate ion.

In general, same trend with the activation energies of first step was observed. EDGs generally decrease the activation barrier as they increase the electron density on C_3 atom and faciliate the C_2 - TfO^- bond cleavage. Activation barriers of EDGs on C_3 atom were similar in the range of 1.3 kcal.mol^{-1}. EWGs have relatively higher activation barriers due to decreased electron density on central carbon atom. Activation barrier increased on β-substituted α-trifloylenamines 7a ($\Delta G^{\ddagger}$ = 3.5 kcal.mol^{-1}) and 8a ($\Delta G^{\ddagger}$ = 5.4 kcal.mol^{-1}) as the electron withdrawing ability of substituent is increased. Activation barrier is even higher in the case of α-trifloylenamine 9a ($\Delta G^{\ddagger}$ = 6.0 kcal.mol^{-1}) which has the most electronegative atom fluorine. Generally, α-substituted ones have higher activation barriers as they are directly bonded to C_3 atom. Although the EWG bearing α-trifloylenamine have closer activation barrier among them, there was a sharp increase on methyl acetate bearing α-trifloylenamine 14a ($\Delta G^{\ddagger}$ = 14.0 kcal.mol^{-1}) followed by α-chlorine substituted 15a ($\Delta G^{\ddagger}$ = 9.7 kcal.mol^{-1}) α-trifloylamine. The expected order was observed between the phenyl ether 12a ($\Delta G^{\ddagger}$ = 7.7 kcal.mol^{-1}), aniline 13a ($\Delta G^{\ddagger}$ = 6.7 kcal.mol^{-1}), and phenyl sulfide 11a ($\Delta G^{\ddagger}$ = 5.8 kcal.mol^{-1}) in contrast to first and second steps. However, the parent structures 16a-18a did not follow the expected trend. Aniline substituted 18a ($\Delta G^{\ddagger}$ = 3.4 kcal.mol^{-1}) α-trifloylenamine have one of the lowest activation barriers among all substituents due to the delocalization that stems from unpaired electrons of nitrogen atom.

In the case of N_1 substituents, same trend was observed with C_3 substituted ones. α-trifloylenamines bearing EDGs have lower activation barrier than EWG substituted α-trifloylenamines. EDGs have similar/closer activation barrier among them except for diallyl substituted one 2b ($\Delta G^{\ddagger} = 6.0$ kcal.mol^{-1}). The size and orientation of 2b might decrease the activation barrier as it hinders the cleavage of TfO - C_2 bond. Energy refinements were performed with range-separated ωB97XD, double hybrid B2PLYP, and hybrid-GGA MPW1K functionals and given in Tables 3.9 and 3.11. In general, energy refinements showed similar trends regardless of the level of theory. Energy profiles are tabulated in Tables A.5 and A.6 and obtained from IRC optimization. Although the energies were calculated from separate reactants, the reaction free energies (ΔG_{rxn}) in Tables 3.9 and 3.10 were calculated according to the product complex, since the presence of ions may lead to BSSE errors.

Table 3.9. Gibbs free energies of activation $\Delta G^{\ddagger}$ and reaction ΔG_{rxn} of N_1 substituted KI's.

		M06-2X		ωB97XD		MPW1K		B2PLYP	
	Amide	$\Delta G^{\ddagger}$	ΔG_{rxn}	$\Delta G^{\ddagger}$	ΔG_{rxn}	$\Delta G^{\ddagger}$	ΔG_{rxn}	$\Delta G^{\ddagger}$	ΔG_{rxn}
1a	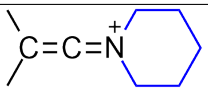	3.1	-4.4	1.2	-6.0	3.7	-2.6	0.9	-9.7
1b	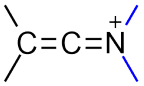	3.9	-5.3	1.7	-7.0	3.5	-4.5	0.4	-11.4
2b	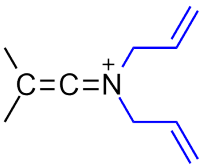	6.0	-1.5	4.1	-3.1	5.2	-1.2	1.6	-8.5
3b	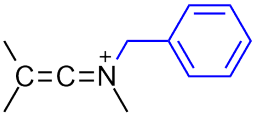	3.6	-6.0	4.2	-2.0	5.8	0.3	1.8	-6.9
4b	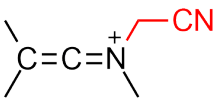	7.4	2.9	5.4	1.6	7.9	4.7	3.9	-2.5
5b	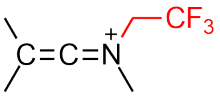	6.8	0.3	4.6	-1.1	6.6	1.4	3.0	-4.9

Table 3.10. Gibbs free energies of activation $\Delta G^{\ddagger}$ and reaction ΔG_{rxn} of C_3 substituted KI's.

	KI	$\Delta G^{\ddagger}$	$\Delta G^{\ddagger}$		KI	$\Delta G^{\ddagger}$	$\Delta G^{\ddagger}$		KI	$\Delta G^{\ddagger}$	$\Delta G^{\ddagger}$
1a	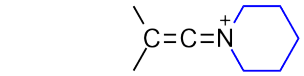	3.9	-5.3	**8a**	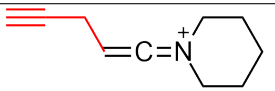	5.4	-2.1	**15a**	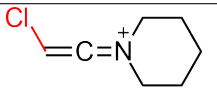	9.7	4.8
2a	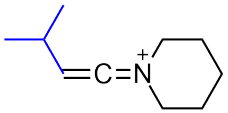	4.0	-4.5	**9a**	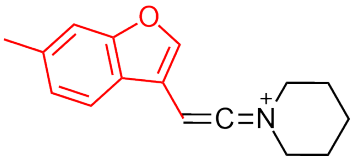	6.5	-0.9	**16a**	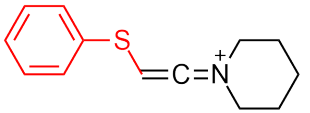	6.8	0.5
3a	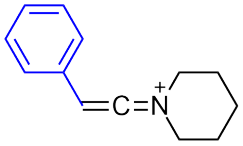	3.3	-5.0	**10a**	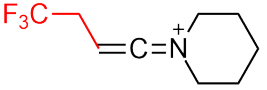	6.0	-2.9	**17a**	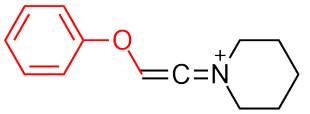	7.3	4.7
4a	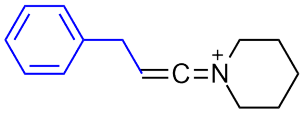	4.6	-4.0	**11a**	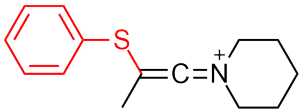	5.8	-1.0	**18a**	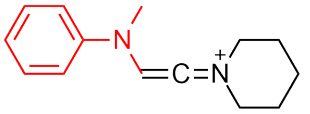	3.4	-4.2
5a	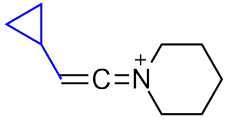	3.3	-5.0	**12a**	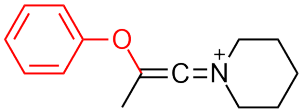	7.7	3.7				
6a	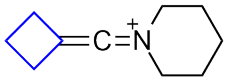	4.0	-4.7	**13a**	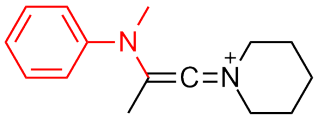	6.7	-5.0				
7a	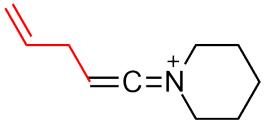	3.5	-7.9	**14a**	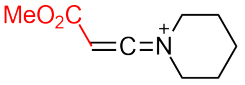	10.4	3.7				

Table 3.11. Free energy barriers ($\Delta G^{\ddagger}$) and reaction free energies (ΔG_{rxn}) for C_3-substituted amides for third step

	M06-2X		ωB97XD		MPW1K		B2PLYP	
Entry	$\Delta G^{\ddagger}$	ΔG_{rxn}	$\Delta G^{\ddagger}$	ΔG_{rxn}	$\Delta G^{\ddagger}$	ΔG_{rxn}	$\Delta G^{\ddagger}$	ΔG_{rxn}
1a	3.9	-5.3	1.7	-7.0	3.5	-4.5	0.4	-11.4
2a	4.0	-4.5	2.0	-6.0	3.0	-3.9	-0.6	-2.0
3a	3.3	-5.0	1.2	-6.8	2.8	-5.5	-0.1	-12.3
4a	3.7	-5.0	1.9	-6.3	3.4	-3.5	0.7	-9.7
5a	3.3	-5.0	1.3	-6.9	3.3	-4.5	1.0	-10.9
6a	4.0	-4.7	2.4	-5.6	4.3	-2.7	2.4	-8.9
7a	3.5	-7.9	1.8	-8.8	3.3	-6.5	1.0	-12.2
8a	5.4	-2.1	3.4	-3.8	4.3	-2.5	1.2	-9.3
9a	6.2	-1.0	4.5	-3.0	6.5	0.2	2.7	-7.4
10a	5.9	-2.9	4.5	-4.0	6.5	-0.6	3.7	-7.6
11a	5.8	-1.0	3.7	-1.7	4.9	0.4	1.6	-6.1
12a	7.7	3.7	6.7	3.8	6.1	4.1	1.7	-3.4
13a	6.7	-5.0	4.2	-9.1	5.7	-5.2	2.1	-12.3
14a	10.4	3.7	8.5	2.0	11.5	4.7	7.6	-3.4
15a	9.7	4.8	7.5	3.9	9.3	6.6	4.8	-0.6
16a	6.8	0.5	4.9	0.1	5.5	2.1	1.1	-5.2
17a	7.3	4.7	5.4	3.4	6.9	5.9	2.3	-1.3
18a	3.4	-4.2	0.6	-7.0	3.4	-4.5	0.3	-11.6

Same trend was observed with substituents on C_3 and N_1; the EDGs have decreased the activation barrier, while EWGs have increased it. The activation energy values of the third step are lower than the first ones. First step is proven to be RDS meaning that the amide reactivity is crucial since the RDS is an electrophilic activation of starting amides. Amide reactivity was investigated in detail in the following sections by means of distortion/interaction, population analysis, and non-covalent interactions.

3.4. Amide Reactivity

The substituent's effect on starting amides were examined to see their contribution to Ghosez's formation reaction with distortion/interaction model analysis, non-covalent interactions and population analysis.

3.4.1. Distortion/Interaction Model Analysis

Distortion/interaction energy analysis were investigated to rationalize the difference in activation barriers of the electrophilic activation step caused by various substituents. According to Table 3.12, distortion mainly influences some part of the activation energies, while interaction affects the remaining ones. The lowest distortion energy ($\Delta E^{\ddagger}_{dist}$) belongs to TS-6a, while TS-12a has the highest distortion energy, therefore, the highest activation barrier. The results are consistent with the activation barriers in Table 3.3. TS-6a is the less crowded TS among all which means its reactants to relatively distort less. Moreover, the results of the ASM model were also in agreement with critical distances of TS structures Figure 3.12. TS-6a has a relatively long critical distance between the carbonyl oxygen and sulfur atom of Tf_2O when compared to TS-11–TS-13a. The short S···O distances in TS-11a, TS-12a, and TS-13a demonstrate the product-like nature of the TS that cause higher distortion energy, and higher free energy of activation. Another notable observation is that the cleavage of S-O bond in Tf_2O follows a reverse trend. The cleaved TfO^- is more distorted when the distances of S-O bond of Tf_2O are longer and as a result, the energy of distortion is increased. Moreover, as previously mentioned, TS-11a has an unexpected activation barrier. TS-11a has higher interaction energy compared to TS-12a and TS-13a, which leads TS-11a to have higher activation energies. In parent counterparts (TS-16a, TS-17a, TS-18a), distortion energies govern the reaction and lowest distortion energy, which leads to lowest activation barrier are seen in TS-16a.

Table 3.12. Distortion and interaction energies for the first step in KI formation reactions with different C_3 and N_1 substituents (M06-2X/6-31+G(d,p), in $CHCl_3$)

C-substituted TS								N-substituted TS			
TS	$\Delta E^{\ddagger}$	$\Delta E^{\ddagger}_{dist}$	$\Delta E^{\ddagger}_{int}$	TS	$\Delta E^{\ddagger}$	$\Delta E^{\ddagger}_{dist}$	$\Delta E^{\ddagger}_{int}$	TS	$\Delta E^{\ddagger}$	$\Delta E^{\ddagger}_{dist}$	$\Delta E^{\ddagger}_{int}$
1a	14.1	39.0	-24.9	**10a**	15.1	38.5	-23.5	**1b**	14.2	37.8	-23.6
2a	11.9	40.4	-28.5	**11a**	16.1	41.6	-25.5	**1a**	14.1	39.0	-24.9
3a	12.1	37.4	-25.3	**12a**	14.0	46.6	-32.6	**2b**	16.1	43.7	-27.1
4a	12.8	41.3	-28.5	**13a**	12.8	44.2	-31.4	**3b**	14.9	40.6	-25.7
5a	12.7	40.3	-27.6	**14a**	13.7	39.7	-26.0	**4b**	17.6	42.7	-25.1
6a	12.2	36.4	-24.2	**15a**	15.2	39.4	-24.2	**5b**	17.3	43.1	-25.8
7a	14.1	37.6	-23.5	**16a**	11.3	37.2	-25.9				
8a	14.2	39.2	-25.0	**17a**	16.0	41.5	-25.5				
9a	13.5	39.0	-25.5	**18a**	12.8	42.3	-29.5				

Table 3.12 also showed that the distortion energies of N-substituted TSs are also in agreement with the activation barriers in Table 3.3. TS-1a and TS-1b have relatively lower distortion energies leading to lower activation barriers. Interaction energies of N-substituted TSs are also similar, excluding TS-1b and TS-2b. Furthermore, relatively short S···O critical distance between amide carbonyl oxygen (4b and 5b) and sulfur of Tf_2O and long S···O distances in the cleavage of Tf_2O give the product-like nature of TSs that result in higher free energies of activation and higher endothermicity (ΔG_{rxn} = 22.6 and 18.7 kcal/mol, respectively) (Figure 3.13).

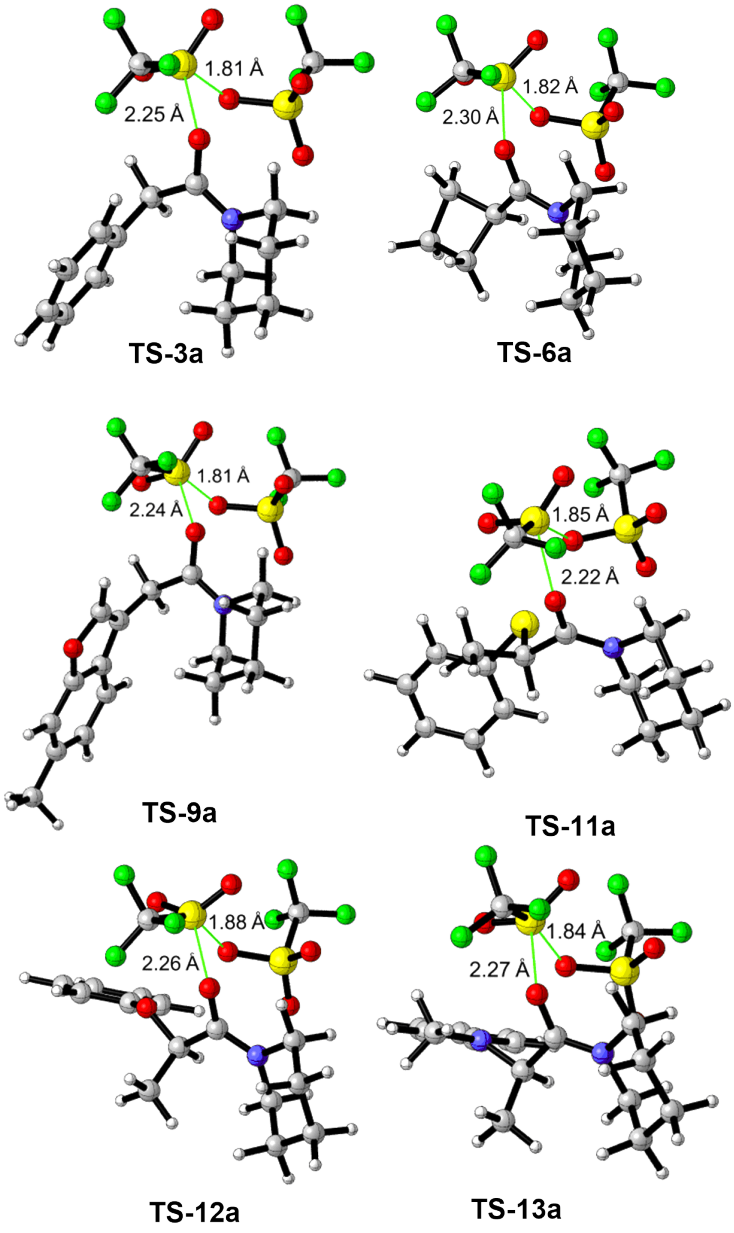

Figure 3.12. Critical distances of optimized TS structures of Ghosez's reaction with selected C-substituted amides.

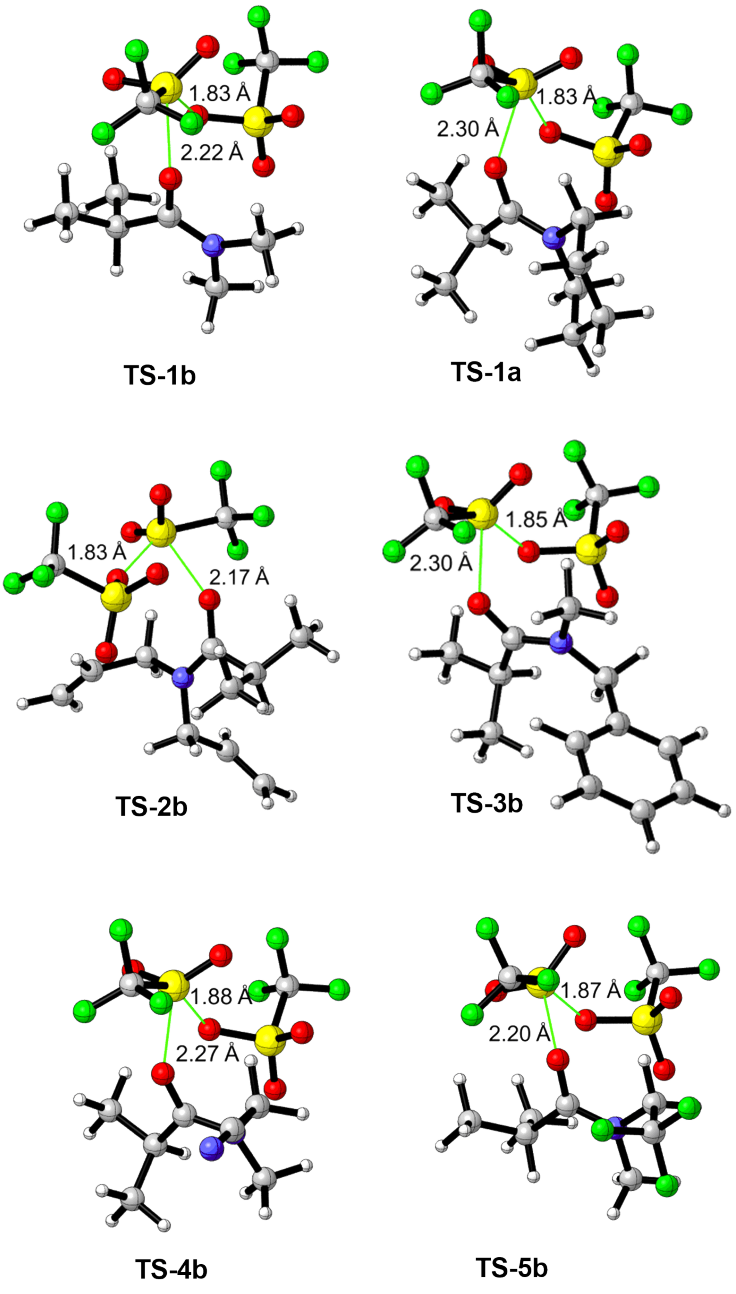

Figure 3.13. Critical distances of optimized N-substituted TS structures.

3.4.2. Non-covalent Interactions

In order to support the energetic and distortion/interaction model results, all of the TS structures were investigated using NCIplot program [75]. Herein, the NCI plots of same selected transition states are discussed. In particular, TS stabilizing interactions such as lone pair-π (lp-π) and CH-π interactions were observed (Figure 3.14). In TS-3a and TS-9a, CH-π interactions were observed. The hydrogens of the piperidine ring interacts with the benzyl (3a) and benzofuran (9a) rings. The CH-π interaction confirms that TS-9a has relatively lower activation barrier among other EWG groups. Non-conventional interactions such as CH···O and CH···F interactions were seen in some TS structures as incoming hydrogens of substituents on C_3 atom interacts with oxygen in TS-5a and TS-9a fluorine atom. Similar interaction energies in TS-6a–TS-8a, and TS-10a were seen in Table 3.12, which is corralated with CH···O interactions. Since TS-5a and TS-9a have extra CH···F interactions, higher interaction energies were observed compared to others.

In addition to previous ones, similar stabilizing interactions were seen from TS-5a to TS-8a, TS-10a and TS-18a as shown in Figure 3.14. The unexpected activation barrier trend that is observed in (Table 3.3) for TS-11a, TS-12a, and TS-13a can also be explained with the NCI effect. TS-12a and TS-13a have relatively lower interaction energies compared to TS-11a that may stem from lone pair-π (lp-π) interactions. TS-11a does not have these stabilizing interactions that results in the unexpected activation barrier trend (Figure 3.14).

When TS-16a–TS-18a are examined, lp-π interactions were observed and this leads to a relatively lower activation barrier and higher interaction energies. Besides, low distortion energies in TS-16a–TS-18a also depicts that the methyl group on C_3 creates steric hindrance and increases the activation barriers.

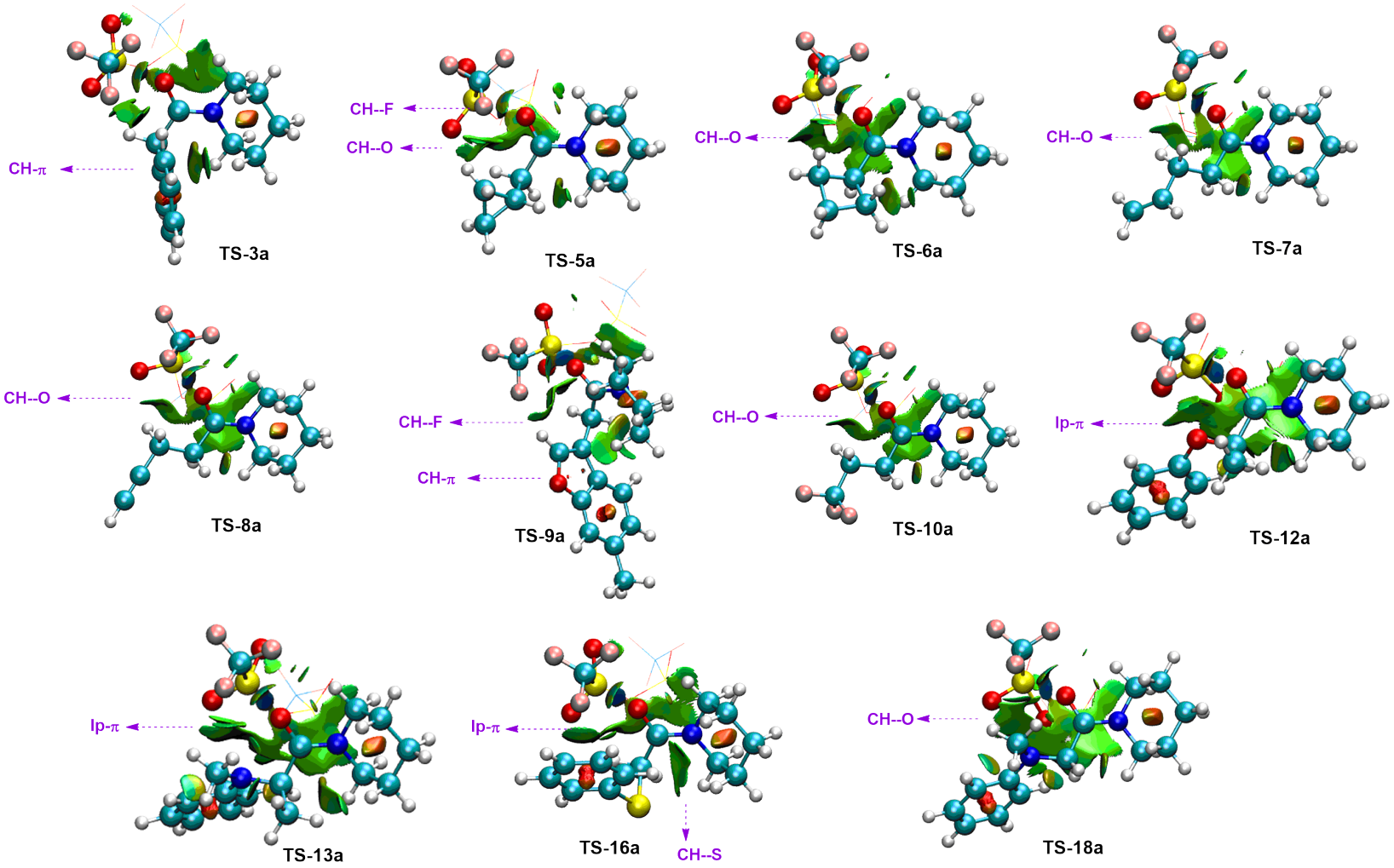

Figure 3.14. Non-covalent interaction (NCI) plots of the TS structures. The NCI isosurface value= 0.5 au using SCF densities.

3.4.3. Population Analysis

Investigation of the substituent effect on reactivity of experimentally accessible amides was tabulated in Tables 3.3 and 3.4 with population analysis. Natural bond orbital (NBO) analysis was performed to clarify the electrostatic nature of the RDS of the formation reaction of KI and rationalize the calculated order of activation barriers. Computed data is displayed in Table 3.13. Natural Population Analysis (NPA) calculations show that for both N_1 and C_3 substituents, electron-donating groups result in higher electron density on the carbonyl oxygen, while electron-withdrawing groups caused lower electron density. When compared 7a, 8a, and 10a with 11a-18a, it is seen that the inductive effect of the vinyl 7a, propargyl 8a, and trifluoromethyl 10a reduced when they are in more distant positions compared to 11a-18a that are adjacent to the carbonyl moiety.

Likewise, the electron density and the NPA atomic charges on carbonyl oxygen are higher for 1b and 1a than in the allyl and benzyl substituted ones, 2b and 3b. Electron density on carbonyl oxygen is decreased when stronger electron-withdrawing groups as nitrile 4b and trifluoromethyl 5b is present. To conclude, the NPA atomic charges presented in Table 3.13 are compatible with the activation energies of the RDS (Tables 3.3 and 3.4).

Table 3.13. NPA atomic charges of C_3 and N_1-substituted amides.

C_3 Substituents					N_1 Substituents				
Entry	C_3	O	C_2	N_1	Entry	C_3	O	C_2	N_1
1a	-0.520	-0.704	0.730	-0.369	**1b**	-0.519	-0.702	0.725	-0.367
2a	-0.522	-0.702	0.729	-0.558	**1a**	-0.520	-0.704	0.730	-0.369
3a	-0.518	-0.700	0.722	-0.571	**2b**	-0.510	-0.699	0.733	-0.369
4a	-0.520	-0.701	0.724	-0.557	**3b**	-0.522	-0.691	0.728	-0.374
5a	-0.520	-0.705	0.724	-0.555	**4b**	-0.518	-0.675	0.738	-0.369
6a	-0.516	-0.701	0.725	-0.367	**5b**	-0.371	-0.680	0.741	-0.536
7a	-0.517	-0.710	0.726	-0.526					
8a	-0.517	-0.700	0.723	-0.556					
9a	-0.516	-0.699	0.725	-0.568					
10a	-0.513	-0.700	0.722	-0.579					
11a	-0.510	-0.688	0.714	-0.477					
12a	-0.506	-0.686	0.711	0.001					
13a	-0.522	-0.693	0.715	-0.139					
14a	-0.519	-0.687	0.723	-0.654					
15a	-0.507	-0.684	0.692	-0.536					
16a	-0.512	-0.691	0.704	-0.687					
17a	-0.507	-0.693	0.679	-0.204					
18a	-0.517	-0.693	0.702	-0.332					

3.5. KI Reactivity

3.5.1. Local Reactivity Descriptors

In order to predict the local reactivity of corresponding KIs and to rationalize the calculated activation barrier order, the electrophilic Parr function $P_k{}^+$ and the Fukui function $f_k{}^+$ were calculated and tabulated in Table 3.14.

Parr and Fukui function analysis emphasize that electrophilicity is relatively lower when substituents with electron-donating ability (KI-3b) through resonance (KI-3a), delocalization (KI-13a and 18a), and mesomeric effect (KI-14a) are present on the C_2 atom. The presence of electron-withdrawing substituents and steric hindrance also affected electrophilicity. KI-10a, KI-4b, and KI-5b have comparatively increased electrophilicity as they carry highly electronegative substituents like nitrile and trifluoromethyl which are strong EWG groups. KIs with X-Phenyl groups have lower electrophilicity compared to other EWG substituted ones due to steric hindrance. Besides, phenyl ether (KI-12a and KI-17a) substituted ones expectedly have higher electrophilicity than phenyl sulfide (KI-11a and KI-16a) and aniline (KI-13a and KI-18a) since oxygen is more electronegative than sulfur and nitrogen. However, aniline substituted KIs have the lowest ${P_k}^+$ and ${f_k}^+$ among all since there is delocalization which reduces electrophilicity. Thus, generally, KIs carrying substituents that have the ability of electron donation and generates steric hindrance have relatively lower electrophilicity. In contrast, KIs that have electron-withdrawing substituents with electronegative atoms on them and relatively smaller in size are more electrophilic and more available to the nucleophilic attacks.

Table 3.14. ${P_k}^+$ and ${f_k}^+$ for the C_2 atoms of corresponding KIs.

C-Substituents						N-Substitutents		
KI	${P_k}^+$	${f_k}^+$	KI	${P_k}^+$	${f_k}^+$	KI	${P_k}^+$	${f_k}^+$
1a	0.702	0.364	**10a**	0.671	0.340	**1b**	0.711	0.368
2a	0.681	0.353	**11a**	0.602	0.290	**1a**	0.702	0.364
3a	0.340	0.161	**12a**	0.659	0.332	**2b**	0.694	0.353
4a	0.683	0.352	**13a**	0.367	0.231	**3b**	0.712	0.364
5a	0.678	0.355	**14a**	0.441	0.210	**4b**	0.736	0.372
6a	0.638	0.356	**15a**	0.556	0.299	**5b**	0.743	0.369
7a	0.680	0.356	**16a**	0.598	0.302			
8a	0.663	0.353	**17a**	0.634	0.338			
9a	0.692	0.309	**18a**	0.144	0.131			

4. CONCLUSION

In conclusion, to give a detailed understanding of KI formation, the energetics of the formation of KI through four different mechanisms were disclosed. Notably, the most commonly used method of Ghosez that includes activation of starting amide with triflic anhydride and followed by treatment with collidine is comprehensively investigated. In the first part, to examine the effect of the substituent on ease of formation of triflated amide (RDS for overall reaction) to give corresponding KI, a set of suitable substituents on the C_3 the N_1 atoms of starting amide are modeled.

Then, all steps of Ghosez's formation reaction were investigated with same set of substituents energetically. Results prove that the first step of the reaction is the RDS meaning that the reactivity of starting amides towards triflic anhydride is directly related to the formation of the KI. In general, EDGs on C_3 and N_1 atoms of starting amide lower the activation barrier as they increase electron density on carbonyl oxygen, while EWGs tend to display a reverse trend as they decrease electron density on carbonyl oxygen and, as a result, increase the activation barrier. Steric hindrance around the starting amide also has a detrimental effect on the activation barrier for the electrophilic activation of the amide with triflic anhydride. Population analysis proves that in general, EDG substituted amides have higher electron density on the oxygen atom of carbonyl rather than EWG substituted ones, which make them more reactive for electrophilic activation by Tf_2O. Distortion/interaction model analysis and the investigation of non-covalent interactions are in agreement with the energetic findings. Lastly, the reactivity analysis was performed on the corresponding KIs to predict the local reactivity. Electrophilicity of the KIs substituted with EDGs or create steric hindrance is relatively lower. KIs carrying EWGs are more available to nucleophilic attacks on C_2 atom. Overall, this computational study provides rationalization of diverse experimental results obtained previously as well as allowing a more detailed prediction of the ease of formation of keteniminium intermediates for synthetic applications.

Bibliography

1. Evano, G., M. Lecomte, P. Thilmany and C. Theunissen, "Keteniminium Ions: Unique and Versatile Reactive Intermediates for Chemical Synthesis", *Synthesis (Germany)*, Vol. 49, No. 15, pp. 3183–3214, 2017.

2. Marchand-Brynaert, J. and L. Ghosez, "Cycloadditions of Keteneimmonium Cations to Olefins and Dienes. A New Synthesis of Four-Membered Rings", *Journal of the American Chemical Society*, Vol. 94, No. 8, pp. 2870–2872, 1972.

3. Ghosez, L., B. Haveaux and H. G. Viehe, "Alkyl and Aryl α-Chloro Enamines", *Angewandte Chemie International Edition in English*, Vol. 8, No. 6, pp. 454–455, 1969.

4. Sidani, A., J. Marchand-Brynaert and L. Ghosez, "A Convenient Procedure for the Synthesis of Cyclobutanones", *Angewandte Chemie International Edition in English*, Vol. 13, No. 4, pp. 267–267, 1974.

5. Falmagne, J. -B.; Escudero, J.; Taleb-Sahraoui, S.; Ghosez, L., "Cyclobutanone and Cyclobutenone Derivatives by Reaction of Tertiary Amides with Alkenes or Alkynes", *Angewandte Chemie International Edition in English*, Vol. 20, pp. 879–880, 1981.

6. Deyrup, J. A. and G. S. Kuta, "Deprotonation of a Hindered Keteniminium Salt", *Journal of Organic Chemistry*, Vol. 43, No. 3, pp. 501–505, 1978.

7. Viehe, H. G., R. Buijle, R. Fuks, R. Merényi and J. M. F. Oth, "Acylation, Alkylation, and Protonation of Alkynylamines", *Angewandte Chemie International Edition in English*, Vol. 6, No. 1, pp. 77–78, 1967.

8. Dekorver, K. A., H. Li, A. G. Lohse, R. Hayashi, Z. Lu, Y. Zhang and R. P. Hsung, "Ynamides: A Modern Functional Group for the New Millennium", *Chemical Re-*

views, Vol. 110, No. 9, pp. 5064–5106, 2010.

9. Zhou, B., T. D. Tan, X. Q. Zhu, M. Shang and L. W. Ye, "Reversal of Regioselectivity in Ynamide Chemistry", *ACS Catalysis*, Vol. 9, No. 7, pp. 6393–6406, 2019.

10. Evano, G., A. Coste and K. Jouvin, "Ynamides: Versatile Tools in Organic Synthesis", *Angewandte Chemie - International Edition*, Vol. 49, No. 16, pp. 2840–2859, 2010.

11. Kaiser, D., A. Bauer, M. Lemmerer and N. Maulide, "Amide Activation: An Emerging Tool For Chemoselective Synthesis", *Chemical Society Reviews*, Vol. 47, No. 21, pp. 7899–7925, 2018.

12. Madelaine, C., V. Valerio and N. Maulide, "Revisiting Keteniminium Salts: More Than the Nitrogen Analogs of Ketenes", *Chemistry - An Asian Journal*, Vol. 6, No. 9, pp. 2224–2239, 2011.

13. B., S. B., "Intramolecular Cycloaddition Reactions of Ketenes and Keteniminium Salts with Alkenes", *Chemical Reviews*, Vol. 88, No. 5, pp. 793–811, 1988.

14. Zhang, Y., R. P. Hsung, X. Zhang, J. Huang, B. W. Slafer and A. Davis, "Brønsted Acid-Catalyzed Highly Stereoselective Arene-ynamide Cyclizations. A Novel Keteniminium Pictet-Spengler Cyclization in Total Syntheses of (±)-desbromoarborescidines A and C", *Organic Letters*, Vol. 7, No. 6, pp. 1047–1050, 2005.

15. Kolleth, A., D. Dagoneau, P. Quinodoz, A. Lumbroso, M. Avanthay, S. Catak, S. Sulzer-Mossé and A. De Mesmaeker, "Synthesis of Benzazepinones via Intramolecular Cyclization Involving Ketene Iminium Intermediates", *Helvetica Chimica Acta*, Vol. 102, No. 9, 2019.

16. Lumbroso, A., J. Behra, A. Kolleth, P. Y. Dakas, U. Karadeniz, S. Catak, S. Sulzer-

Mossé and A. De Mesmaeker, "Access to Functionalized 3-amino-benzothiophenes Using Keteniminium Intermediates", *Tetrahedron Letters*, Vol. 56, No. 47, pp. 6541–6545, 2015.

17. Villedieu-Percheron, E., S. Catak, D. Zurwerra, R. Staiger, M. Lachia and A. De Mesmaeker, "$6\pi/10\pi$-Electrocyclization of Ketene-iminium Salts for the Synthesis of Substituted Naphthylamines", *Tetrahedron Letters*, 2014.

18. Kolleth, A., S. Müller, A. Lumbroso, G. Tanriver, S. Catak, S. Sulzer-Mossé and A. De Mesmaeker, "Access to 3-aminobenzothiophenes and 3-aminothiophenes Fused to 5-membered heteroaromatic Rings Through 6π-electrocyclization Reaction of Keteniminium Salts", *Tetrahedron Letters*, 2018.

19. Tanriver, G., D. Dagoneau, U. Karadeniz, A. Kolleth, A. Lumbroso, S. Sulzer-Mossé, A. De Mesmaeker and S. Catak, "Keteniminium Salts: Reactivity and Propensity toward Electrocyclization Reactions", *The Journal of Organic Chemistry*, Vol. 85, No. 2, pp. 449–463, jan 2020.

20. Dagoneau, D., A. Kolleth, A. Lumbroso, G. Tanriver, S. Catak, S. Sulzer-Mossé and A. De Mesmaeker, "Straightforward Synthesis of 3-Aminothiophenes Using Activated Amides", *Helvetica Chimica Acta*, Vol. 102, No. 4, 2019.

21. Dagoneau, D., A. Kolleth, P. Quinodoz, G. Tanriver, S. Catak, A. Lumbroso, S. Sulzer-Mossé and A. De Mesmaeker, "Keteniminium Salts as Key Intermediates for the Efficient Synthesis of 3-Amino-Indoles and -Benzofurans", *Helvetica Chimica Acta*, Vol. 103, No. 1, p. e1900217, 2020.

22. Hoornaert, C., A. M. Hesbain-Frisque and L. Ghosez, "Cyclobutenylideneammonium Salts from the Cycloadditions of Keteniminium Salts to Acetylenes", *Angewandte Chemie International Edition in English*, Vol. 14, No. 8, pp. 569–570, 1975.

23. Brady, W. T., Y. S. F. Giang, L. Weng and M. M. Dad, "Intramolecular [2 + 2] Cycloadditions of Ketene Iminium Salts to Carbon-Carbon Double Bonds", *Journal*

of Organic Chemistry, Vol. 52, No. 11, pp. 2216–2220, 1987.

24. Deyrup, J. A. and W. A. Szabo, "Deprotonation of Ternary Iminium Salts", *Journal of Organic Chemistry*, Vol. 40, No. 14, pp. 2048–2052, 1975.

25. Stang, P. J., Hanack, M., Subramanian, L. R., "Perfluoroalkanesulfonic Esters: Methods of Preparation and Applications in Organic Chemistry", *Synthesis*, Vol. 2, pp. 85–126, 1982.

26. Zificsak, C. A., J. A. Mulder, R. P. Hsung, C. Rameshkumar and L. L. Wei, "Recent Advances in the Chemistry of Ynamines and Ynamides", *Tetrahedron*, Vol. 57, pp. 7575–7606, 2001.

27. Lecomte, M. and G. Evano, "Harnessing the Electrophilicity of Keteniminium Ions: A Simple and Straightforward Entry to Tetrahydropyridines and Piperidines from Ynamides", *Angewandte Chemie - International Edition*, Vol. 55, No. 14, pp. 4547–4551, 2016.

28. Born, M. and R. Oppenheimer, "Zur Quantentheorie der Molekeln", *Annalen der Physik*, Vol. 389, No. 20, pp. 457–484, 1927.

29. Engel, E. and R. M. Dreizler, *Density Functional Theory Theoretical and Mathematical Physics*, Springer-Verlag Berlin Heidelberg, 2011.

30. Becke, A. D., "A new mixing of Hartree–Fock and local density functional theories", *The Journal of Chemical Physics*, Vol. 98, No. 2, pp. 1372–1377, 1993.

31. Becke, A. D., "Density Functional Exchange Energy Approximation with Correct Asymptotic Behavior", *Physical Review A*, Vol. 38, pp. 3098–3100, Sep 1988.

32. Hohenberg, P. and W. Kohn, "Inhomogeneous Electron Gas", *Physical Review*, Vol. 136, pp. B864–B871, Nov 1964.

33. Kohn, W. and L. J. Sham, "Self-Consistent Equations Including Exchange and

Correlation Effects", *Physical Review*, Vol. 140, pp. A1133–A1138, Nov 1965.

34. Perdew, J. P., K. Burke and M. Ernzerhof, "Generalized Gradient Approximation Made Simple", *Physical Review Letters*, Vol. 77, pp. 3865–3868, Oct 1996.

35. Zhao, Y. and D. G. Truhlar, "The M06 Suite of Density Functionals for Main Group Thermochemistry, Thermochemical Kinetics, Noncovalent Interactions, Excited States, and Transition Elements: Two New Functionals and Systematic Testing of Four M06-class Functionals and 12 Other Function", *Theoretical Chemistry Accounts*, Vol. 120, No. 1-3, pp. 215–241, 2008.

36. Zhao, Y. and D. G. Truhlar, "A New Local Density Functional for Main-Group Thermochemistry, Transition Metal Bonding, Thermochemical Kinetics, and Noncovalent Interactions", *Journal of Chemical Physics*, Vol. 125, No. 19, pp. 1–61, 2006.

37. Vydrov, O. A. and G. E. Scuseria, "Assessment of A Long-Range Corrected Hybrid Functional", *The Journal of Chemical Physics*, Vol. 125, No. 23, p. 234109, 2006.

38. Chai, J.-D. and M. Head-Gordon, "Long-Range Corrected Hybrid Density Functionals with Damped Atom-Atom Dispersion Corrections", *Physical Chemistry Chemical Physics*, Vol. 10, No. 1, 6 2008.

39. Slater, J. C., "Atomic Shielding Constants", *Physical Review*, Vol. 36, pp. 57–64, Jul 1930.

40. Ditchfield, R., W. J. Hehre and J. A. Pople, "Self Consistent Molecular Orbital Methods. IX. An Extended Gaussian Type Basis for Molecular Orbital Studies of Organic Molecules", *The Journal of Chemical Physics*, Vol. 54, No. 2, pp. 724–728, 1971.

41. Miertuš, S., E. Scrocco and J. Tomasi, "Electrostatic Interaction of A Solute With A continuum. A Direct Utilizaion of AB Initio Molecular Potentials for the Previ-

sion of Solvent Effects", *Chemical Physics*, Vol. 55, No. 1, pp. 117–129, 1981.

42. van Zeist, W.-J. and F. M. Bickelhaupt, "The Activation Strain Model of Chemical Reactivity", *Organic Biomolecular Chemistry*, Vol. 8, No. 14, pp. 3118–3127, 2010.

43. Fernández, I. and F. M. Bickelhaupt, "The Activation Strain Model and Molecular Orbital Theory: Understanding and Designing Chemical Reactions", *Chemical Society Reviews*, Vol. 43, No. 14, pp. 4953–4967, 2014.

44. Bickelhaupt, F. M. and K. N. Houk, "Analyzing Reaction Rates with the Distortion/Interaction-Activation Strain Model", *Angewandte Chemie International Edition*, Vol. 56, No. 34, pp. 10070–10086, 2017.

45. Dkhissi, A., M. F. Reyniers and G. B. Marin, "A Theoretical Study of Standard Heat of Formation of Systems Involving in the Zinc Reduction of Silicon Tetrachloride", *Theoretical Chemistry Accounts*, Vol. 134, No. 1, 2014.

46. Leach, A., *Molecular Modelling Principles and Applications*, Prentice Hall, England, 2001.

47. Mulliken, R. S., "Electronic Population Analysis on LCAO–MO Molecular Wave Functions. I", *The Journal of Chemical Physics*, Vol. 23, No. 10, pp. 1833–1840, 1955.

48. Löwdin, P. O., "On the Non Orthogonality Problem Connected with the Use of Atomic Wave Functions in the Theory of Molecules and Crystals", *The Journal of Chemical Physics*, Vol. 18, No. 3, pp. 365–375, 1950.

49. Reed, A. E. and F. Weinhold, "Natural Localized Molecular Orbitals", *The Journal of Chemical Physics*, Vol. 83, No. 4, pp. 1736–1740, 1985.

50. Parr, R. G. and W. Yang, "Density-Functional Theory of the Electronic Structure of Molecules", *Annual Review of Physical Chemistry*, Vol. 46, No. 1, pp. 701–728,

1995.

51. Domingo, L. R., M. Ríos-Gutiérrez and P. Pérez, "Applications of the Conceptual Density Functional Theory Indices to Organic Chemistry Reactivity", *Molecules*, Vol. 21, No. 6, 2016.

52. Domingo, L. R., E. Chamorro and P. Pérez, "Understanding the Reactivity of Captodative Ethylenes in Polar Cycloaddition Reactions. A Theoretical Study", *The Journal of Organic Chemistry*, Vol. 73, No. 12, pp. 4615–4624, 2008.

53. Kohn, W. and L. J. Sham, "Self-Consistent Equations Including Exchange and Correlation Effects", *Physical Review*, Vol. 140, pp. A1133–A1138, Nov 1965.

54. Parr, R. G. and W. Yang, "Density Functional Approach to the Frontier-Electron Theory of Chemical Reactivity", *Journal of the American Chemical Society*, Vol. 106, No. 14, pp. 4049–4050, 1984.

55. Yang, W. and W. J. Mortier, "The Use of Global and Local Molecular Parameters for the Analysis of the Gas-Phase Basicity of Amines", *Journal of the American Chemical Society*, Vol. 108, No. 19, pp. 5708–5711, 1986.

56. Domingo, L. R., P. Pérez and J. A. Sáez, "Understanding the Local Reactivity In Polar Organic Reactions Through Electrophilic and Nucleophilic Parr Functions", *RSC Advances*, Vol. 3, No. 5, pp. 1486–1494, 2013.

57. Chamorro, E., P. Pérez and L. R. Domingo, "On the Nature of Parr Functions to Predict the Most Reactive Sites Along Organic Polar Reactions", *Chemical Physics Letters*, Vol. 582, pp. 141–143, 2013.

58. Domingo, L. R., M. J. Aurell, P. Pérez and R. Contreras, "Quantitative Characterization of the Local Electrophilicity of Organic Molecules. Understanding the Regioselectivity on Diels−Alder Reactions", *The Journal of Physical Chemistry A*, Vol. 106, No. 29, pp. 6871–6875, 2002.

59. Pérez, P., L. R. Domingo, M. Duque-Noreña and E. Chamorro, "A Condensed-to-Atom Nucleophilicity Index. An Application to the Director Effects on the Electrophilic Aromatic Substitutions", *Journal of Molecular Structure: THEOCHEM*, Vol. 895, No. 1, pp. 86–91, 2009.

60. Zhao, Y. and D. G. Truhlar, "Density Functionals with Broad Applicability in Chemistry", *Accounts of Chemical Research*, Vol. 41, No. 2, pp. 157–167, 2008.

61. Hermosilla, L., S. Catak, V. V. Speybroeck, M. Waroquier, J. Vandenbergh, F. Motmans, P. Adriaensens, L. Lutsen, T. Cleij and D. Vanderzande, "Kinetic and Mechanistic Study on p-Quinodimethane Formation in the Sulfinyl Precursor Route for the Polymerization of Poly(p-phenylenevinylene)(PPV)", *Macromolecules*, Vol. 43, No. 18, pp. 7424–7433, 2010.

62. Schuchardt, K. L., B. T. Didier, T. Elsethagen, L. Sun, V. Gurumoorthi, J. Chase, J. Li, T. L. Windus and T. Schuchardt, K.L., Didier, B.T., Elsethagen, T., Sun, L., Gurumoorthi, V., Chase, J., Li, J., and Windus, "Basis Set Exchange: A Community Database for Computational Sciences", *Journal of Chemical Information and Modeling*, Vol. 47, No. 3, pp. 1045–1052, 2007.

63. Catak, S., K. Hemelsoet, L. Hermosilla, M. Waroquier and V. Van Speybroeck, "Competitive reactions of organophosphorus radicals on coke surfaces", *Chemistry - A European Journal*, Vol. 17, No. 43, pp. 12027–12036, 2011.

64. Goossens, H., J. M. Winne, S. Wouters, L. Hermosilla, P. J. De Clercq, M. Waroquier, V. Van Speybroeck and S. Catak, "Possibility of [1,5] Sigmatropic Shifts In Bicyclo[4.2.0]octa-2,4-dienes", *Journal of Organic Chemistry*, Vol. 80, No. 5, pp. 2609–2620, 2015.

65. Frisch, M. J., G. W. Trucks, H. B. Schlegel, G. E. Scuseria, M. A. Robb, J. R. Cheeseman, G. Scalmani, V. Barone, G. A. Petersson, H. Nakatsuji and et al., "Gaussian 16 Revision A.03", *Gaussian Inc. Wallingford CT*, 2016.

66. Gonzalez, C. and H. B. Schlegel, "An Improved Algorithm for Reaction Path Following", *The Journal of Chemical Physics*, Vol. 90, No. 4, pp. 2154–2161, 1989.

67. Gonzalez, C. and H. B. Schlegel, "Reaction path following in mass-weighted internal coordinates", *The Journal of Physical Chemistry*, Vol. 94, No. 14, pp. 5523–5527, 1990.

68. Tomasi, J., B. Mennucci and R. Cammi, "Quantum Mechanical Continuum Solvation Models", *Chemical Reviews*, Vol. 105, No. 8, pp. 2999–3094, 2005.

69. Grimme, S., "Semiempirical Hybrid Density Functional with Perturbative Second-order Correlation", *Journal of Chemical Physics*, Vol. 124, No. 3, 2006.

70. Lynch, B. J., P. L. Fast, M. Harris and D. G. Truhlar, "Adiabatic Connection for Kinetics", *Journal of Physical Chemistry A*, Vol. 104, No. 21, pp. 4813–4815, 2000.

71. Lumbroso, A., S. Catak, S. Sulzer-Mossé and A. De Mesmaeker, "Synthesis of Cyclobuteniminium Salts Derived From Aldo-Keteniminium Salts and Study of Their Reactivity in Diels-Alder Reaction", *Tetrahedron Letters*, 2014.

72. Kolleth, A., A. Lumbroso, G. Tanriver, S. Catak, S. Sulzer-Mossé and A. De Mesmaeker, "Synthesis of 4-membered Ring Alkaloid Analogues via Intramolecular [2+2] Cycloaddition Involving Keteniminium Salt Intermediates", *Tetrahedron Letters*, Vol. 58, No. 30, pp. 2904–2909, 2017.

73. Teskey, C. J., P. Adler, C. R. Gonçalves and N. Maulide, "Chemoselective α,β-Dehydrogenation of Saturated Amides", *Angewandte Chemie - International Edition*, Vol. 58, No. 2, pp. 447–451, 2019.

74. Battilocchio, C., G. Iannucci, S. Wang, E. Godineau, A. Kolleth, A. De Mesmaeker and S. V. Ley, "Flow Synthesis of Cyclobutanones via [2 + 2] Cycloaddition of Keteneiminium Salts and Ethylene gas", *React. Chem. Eng.*, Vol. 2, pp. 295–298, 2017.

75. Contreras-García, J., E. R. Johnson, S. Keinan, R. Chaudret, J.-P. Piquemal, D. N. Beratan and W. Yang, "NCIPLOT: A Program for Plotting Noncovalent Interaction Regions", *Journal of Chemical Theory and Computation*, Vol. 7, No. 3, pp. 625–632, 2011.

Appendix A: ENERGY PROFILES FOR GHOSEZ'S MECHANISM

Table A.1. Gibbs free energies of C_3-substituted amides for RDS (M06-2X/6-31+G(d,p)) in CH_3Cl and CH_2Cl_2 for 7a and 10a.

Entry	**R**	**PRC**	**TS**	**PC**	**P**	**Entry**	**R**	**PRC**	**TS**	**PC**	**P**
1a	0.0	4.8	29.8	-3.9	9.2	**11a**	0.0	6.5	32.2	2.7	13.1
2a	0.0	6.8	27.9	-5.8	7.5	**12a**	0.0	5.6	30.9	0.2	11.7
3a	0.0	6.8	28.0	-5.7	8.9	**13a**	0.0	6.7	30.5	-0.4	9.2
4a	0.0	7.9	28.6	-4.7	8.5	**14a**	0.0	5.8	28.5	-3.1	12.5
5a	0.0	5.9	27.7	-6.2	5.5	**15a**	0.0	5.3	29.7	-1.7	14.9
6a	0.0	7.0	27.9	-4.9	6.7	**16a**	0.0	5.3	28.8	-3.8	7.7
7a	0.0	6.3	29.6	-4.0	1.2	**17a**	0.0	6.6	30.1	1.7	12.3
8a	0.0	6.2	30.5	-1.1	11.1	**18a**	0.0	5.8	29.5	-2.9	7.8
9a	0.0	5.5	27.8	-4.5	10.7						
10a	0.0	7.4	31.3	1.2	4.8						

Table A.2. Gibbs free energies of N_1-substituted amides for RDS (M06-2X/6-31+G(d,p)) in CH_3Cl.

Entry	**R**	**PRC**	**TS**	**PC**	**P**
1b	0.0	6.0	30.1	-1.8	9.9
1a	0.0	4.8	29.9	-3.9	9.2
2b	0.0	6.7	32.6	-0.4	11.1
3b	0.0	6.1	32.1	-1.0	11.4
4b	0.0	5.6	33.5	5.3	22.6
5b	0.0	6.0	33.7	3.9	18.7

Table A.3. Gibbs free energies of C_3-substituted enamines for second step of Ghosez's mechanism (M06-2X/6-31+G(d,p)) in CH_3Cl and CH_2Cl_2 for 7a and 10a.

KI	**R**	**PRC**	**TS**	**PC**	**P**	**KI**	**R**	**PRC**	**TS**	**PC**	**P**
1a	0.0	6.2	16.6	-15.8	-1.1	**10a**	0.0	-3.0	7.0	3.5	-12.5
2a	0.0	4.2	18.4	-0.7	-10.6	**11a**	0.0	2.9	13.7	-11.0	-18.6
3a	0.0	1.6	8.3	-2.2	-14.0	**12a**	0.0	-0.4	14.0	-5.2	-14.4
4a	0.0	3.5	11.8	0.6	-10.6	**13a**	0.0	1.3	9.7	-3.8	-12.8
5a	0.0	9.6	11.9	-4.3	-9.8	**14a**	0.0	1.8	5.4	-12.6	-18.4
6a	0.0	3.8	13.5	2.1	-10.4	**15a**	0.0	3.7	8.3	-8.3	-15.5
7a	0.0	8.4	14.8	-0.1	-6.4	**16a**	0.0	9.6	12.4	-3.7	-11.4
8a	0.0	3.7	8.7	-0.6	-11.4	**17a**	0.0	-0.8	6.0	-11.4	-14.4
9a	0.0	2.5	9.4	0.1	-14.6	**18a**	0.0	1.3	9.7	-3.8	-12.8

Table A.4. Gibbs free energies of N_1-substituted enamines for second step of Ghosez's mechanism (M06-2X/6-31+G(d,p)) in CH_3Cl

Entry	**R**	**PRC**	**TS**	**PC**	**P**
1b	0.0	2.8	14.1	-2.3	-16.8
1a	0.0	6.2	16.6	-1.1	-15.8
2b	0.0	5.0	17.8	-0.5	-17.7
3b	0.0	0.7	17.8	0.2	-16.9
4b	0.0	4.1	10.2	-28.5	-15.1
5b	0.0	5.3	14.2	-10.5	-23.4

Table A.5. Gibbs free energies of C_3-substituted KIs (M06-2X/6-31+G(d,p)) in CH_3Cl and CH_2Cl_2 for 7a and 10a.

Entry	**R**	**PRC**	**TS**	**PC**	**P**	**Entry**	**R**	**PRC**	**TS**	**PC**	**P**
1a	0.0	0.6	3.9	-5.3	4.6	**11a**	0.0	0.5	5.8	-1.0	34
2a	0.0	0.8	4.0	-4.5	4.3	**12a**	0.0	3.7	7.7	3.7	9.4
3a	0.0	0.1	3.3	-5.0	5.6	**13a**	0.0	0.1	6.7	-5.0	3.0
4a	0.0	0.3	4.6	-4.0	5.6	**14a**	0.0	2.6	10.4	3.7	16.0
5a	0.0	0.5	3.3	-5.0	5.2	**15a**	0.0	1.0	9.7	4.8	14.5
6a	0.0	1.0	4.0	-4.7	5.7	**16a**	0.0	1.9	6.8	0.5	34.1
7a	0.0	0.0	3.5	-7.9	-4.8	**17a**	0.0	-1.7	7.3	4.7	12.8
8a	0.0	1.0	5.4	-2.1	7.1	**18a**	0.0	-0.3	3.4	-4.2	4.4
9a	0.0	2.8	6.5	-0.9	10.6						
10a	0.0	2.9	6.0	-2.9	0.2						

Table A.6. Gibbs free energies of N_1-substituted KIs (M06-2X/6-31+G(d,p)) in CH_3Cl.

Entry	**R**	**PRC**	**TS**	**PC**	**P**
1a	0.0	0.4	3.1	-4.4	4.5
1b	0.0	0.6	3.9	-5.3	4.6
2b	0.0	0.0	6.0	-1.5	7.4
3b	0.0	-0.4	3.6	-6.0	4.6
4b	0.0	0.7	7.4	2.9	15.5
5b	0.0	0.8	6.8	0.3	13.8

Appendix B: NCI PLOTS

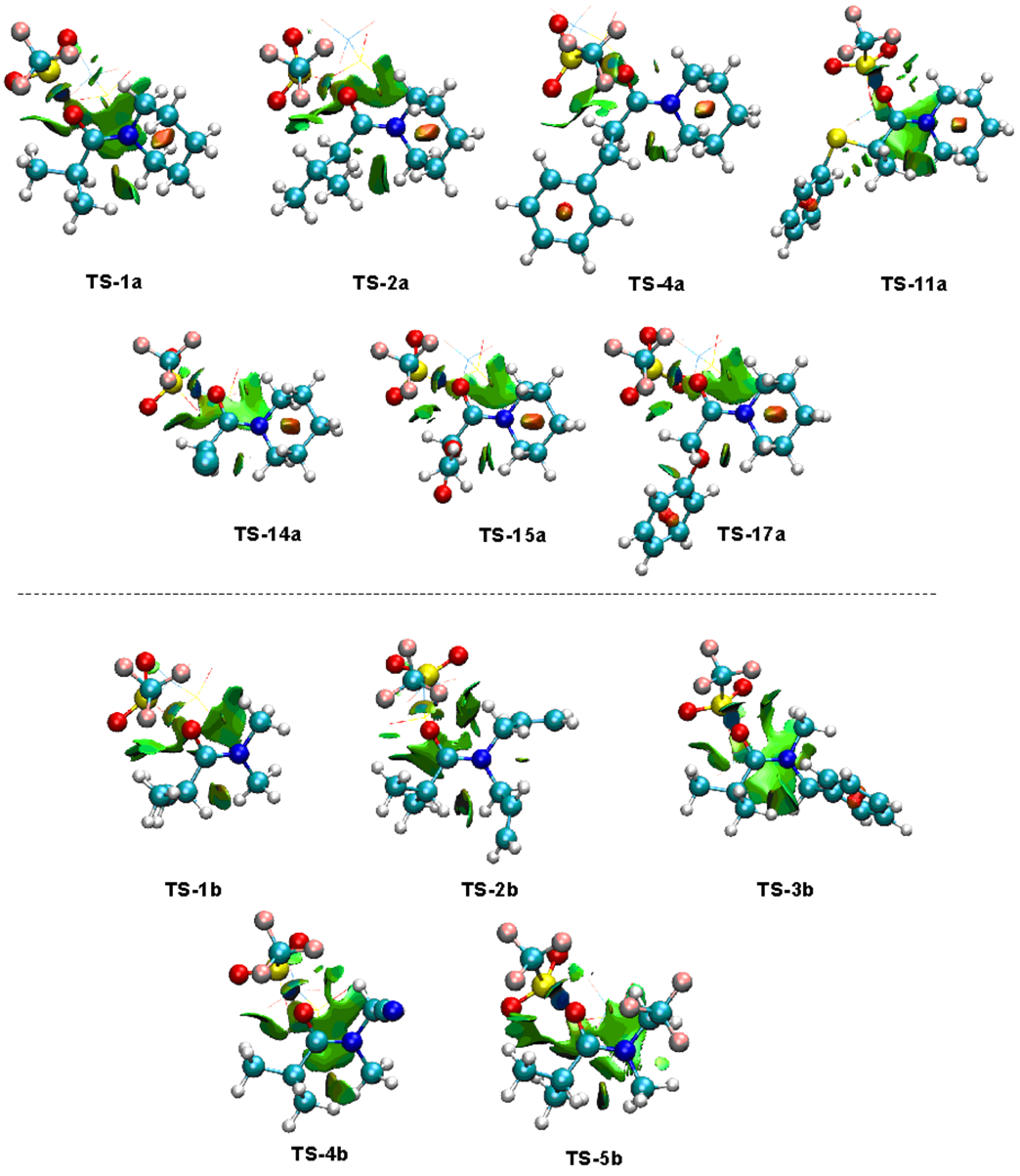

Figure B.1. Non-covalent interaction (NCI) plots for the TS structures of second and third steps. The NCI isosurface value= 0.5 au using SCF densities.

Appendix C: COPY-RIGHT LIST

C.1. The License for Figure 1.1 - Figure 1.7

GEORG THIEME VERLAG KG ORDER DETAILS
Aug 03, 2021

This Agreement between Zeynep Aktaş ("You") and Georg Thieme Verlag KG ("Georg Thieme Verlag KG") consists of your order details and the terms and conditions provided by Georg Thieme Verlag KG and Copyright Clearance Center.

Order Number	501667982
Order date	Jul 19, 2021
Licensed Content Publisher	Georg Thieme Verlag KG
Licensed Content Publication	Synthesis
Licensed Content Title	Keteniminium Ions: Unique and Versatile Reactive Intermediates for Chemical Synthesis
Licensed Content Author	Gwilherm Evano, Morgan Lecomte, Pierre Thilmany, Cédric Theunissen
Licensed Content Date	Jan 1, 2017
Licensed Content Volume	49
Licensed Content Issue	15
Type of Use	Dissertation/Thesis
Requestor type	non-commercial (non-profit)
Format	print and electronic
Portion	figures/tables/images
Number of figures/tables/images	2
Will you be translating?	no
Distribution quantity	1
Title	FORMATION OF KETENIMINIUM SALTS: MECHANISTIC ASPECTS AND EFFECT OF SUBSTITUENTS

Cycloadditions of keteneimmonium cations to olefins and dienes. New synthesis of four-membered rings

Author: Jacqueline Marchand-Brynaert, Leon Ghosez
Publication: Journal of the American Chemical Society
Publisher: American Chemical Society
Date: Apr 1, 1972

JOHN WILEY AND SONS LICENSE
TERMS AND CONDITIONS

Aug 03, 2021

This Agreement between Boğaziçi University -- Zeynep Aktaş ("You") and John Wiley and Sons ("John Wiley and Sons") consists of your license details and the terms and conditions provided by John Wiley and Sons and Copyright Clearance Center.

License Number	5112551399601
License date	Jul 19, 2021
Licensed Content Publisher	John Wiley and Sons
Licensed Content Publication	Angewandte Chemie International Edition
Licensed Content Title	Alkyl and Aryl α-Chloro Enamines
Licensed Content Author	H. G. Viehe, B. Haveaux, L. Ghosez
Licensed Content Date	Dec 17, 2003

JOHN WILEY AND SONS LICENSE
TERMS AND CONDITIONS

Aug 03, 2021

This Agreement between Boğaziçi University -- Zeynep Aktaş ("You") and John Wiley and Sons ("John Wiley and Sons") consists of your license details and the terms and conditions provided by John Wiley and Sons and Copyright Clearance Center.

License Number	5112560110096
License date	Jul 19, 2021
Licensed Content Publisher	John Wiley and Sons
Licensed Content Publication	Angewandte Chemie International Edition
Licensed Content Title	A Convenient Procedure for the Synthesis of Cyclobutanones
Licensed Content Author	Léon Ghosez, Jacqueline Marchand-Brynaert, Abdul Sidani
Licensed Content Date	Dec 22, 2003

JOHN WILEY AND SONS LICENSE
TERMS AND CONDITIONS

Aug 03, 2021

This Agreement between Boğaziçi University -- Zeynep Aktaş ("You") and John Wiley and Sons ("John Wiley and Sons") consists of your license details and the terms and conditions provided by John Wiley and Sons and Copyright Clearance Center.

License Number	5112560285682
License date	Jul 19, 2021
Licensed Content Publisher	John Wiley and Sons
Licensed Content Publication	Angewandte Chemie International Edition
Licensed Content Title	Cyclobutanone and Cyclobutenone Derivatives by Reaction of Tertiary Amides with Alkenes or Alkynes
Licensed Content Author	Léon Ghosez, Sofia Taleb-Sahraoui, José Escudero, et al
Licensed Content Date	Dec 22, 2003

Deprotonation of a hindered keteniminium salt

Author: James A. Deyrup, George S. Kuta
Publication: The Journal of Organic Chemistry
Publisher: American Chemical Society
Date: Feb 1, 1978

JOHN WILEY AND SONS LICENSE
TERMS AND CONDITIONS

Aug 03, 2021

This Agreement between Boğaziçi University -- Zeynep Aktaş ("You") and John Wiley and Sons ("John Wiley and Sons") consists of your license details and the terms and conditions provided by John Wiley and Sons and Copyright Clearance Center.

License Number	5112560929782
License date	Jul 19, 2021
Licensed Content Publisher	John Wiley and Sons
Licensed Content Publication	Angewandte Chemie International Edition
Licensed Content Title	Acylation, Alkylation, and Protonation of Alkynylamines
Licensed Content Author	J. M. F. Oth, R. Merényi, R. Fuks, et al
Licensed Content Date	Dec 17, 2003

JOHN WILEY AND SONS LICENSE
TERMS AND CONDITIONS

Aug 03, 2021

This Agreement between Boğaziçi University -- Zeynep Aktaş ("You") and John Wiley and Sons ("John Wiley and Sons") consists of your license details and the terms and conditions provided by John Wiley and Sons and Copyright Clearance Center.

License Number	5121520374429
License date	Aug 03, 2021
Licensed Content Publisher	John Wiley and Sons
Licensed Content Publication	Angewandte Chemie International Edition
Licensed Content Title	Ynamides: Versatile Tools in Organic Synthesis
Licensed Content Author	Gwilherm Evano, Alexis Coste, Kévin Jouvin
Licensed Content Date	Mar 30, 2010

Issue 21, 2018

Previous Article Next Article

From the journal:
Chemical Society Reviews

Amide activation: an emerging tool for chemoselective synthesis

Daniel Kaiser, [a] Adriano Bauer, [a] Miran Lemmerer [a] and Nuno Maulide [a]*

Author affiliations

Abstract

It is textbook knowledge that carboxamides benefit from increased stabilisation of the electrophilic carbonyl carbon when compared to other carbonyl and carboxyl derivatives. This results in a considerably reduced reactivity towards nucleophiles. Accordingly, a perception has been developed of amides as significantly less useful functional handles than their ester and acid chloride counterparts. However, a significant body of research on the selective activation of amides to achieve powerful transformations under mild conditions has emerged over the past decades. This review article aims at placing electrophilic amide activation in both a historical context and in that of natural product synthesis, highlighting the synthetic applications and the potential of this approach.